Biomechanics and Modeling in Mechanobiology (2021) 20:2227–2245
https://doi.org/10.1007/s10237-021-01503-y

ORIGINAL PAPER

Erythrocyte flow through the interendothelial slits of the splenic venous sinus

Ming Dao[1] · **Ian MacDonald**[2] · **R. J. Asaro**[3]

Received: 23 April 2021 / Accepted: 12 July 2021 / Published online: 18 September 2021

Abstract

The flow patterns of red blood cells through the spleen are intimately linked to clearance of senescent RBCs, with clearance principally occurring within the open flow through the red pulp and slits of the venous sinus system that exists in humans, rats, and dogs. Passage through interendothelial slits (IESs) of the sinus has been shown by MacDonald et al. (Microvasc Res 33:118–134, 1987) to be mediated by the caliber, i.e., slit opening width, of these slits. IES caliber within a given slit of a given sinus section has been shown to operate in an asynchronous manner. Here, we describe a model and simulation results that demonstrate how the supporting forces exerted on the sinus by the reticular meshwork of the red pulp, combined with asymmetrical contractility of stress fibers within the endothelial cells comprising the sinus, describe this vital and intriguing behavior. These results shed light on the function of the sinus slits in species such as humans, rats, and dogs that possess sinusoidal sinuses. Instead of assuming a passive mechanical filtering mechanism of the IESs, our proposed model provides a mechanically consistent explanation for the dynamically modulated IES opening/filtering mechanism observed in vivo. The overall perspective provided is also consistent with the view that IES passage serves as a self-protective mechanism in RBC vesiculation and inclusion removal.

Keywords Splenic flow in human spleens · Flow through venous slits · Operation of the venous slit caliber

1 Introduction

Erythrocytes undergo extensive transit via the macro- and microvascular throughout their, roughly, 120 day lifespan (Alberts et al. 2002; Mebius and Kraal 2005; Lutz 2004; Bosman et al. 2005). During this, they participate in continuous redox reactions fulfilling their primary functions of delivering oxygen and carbon dioxide from and to the lungs from target cells and tissue, respectively. It is no wonder, therefore, that given the energetic reactions that occur within these "simple cells" that oxidative and hence structural molecular damage would accumulate and eventually render the cells nonoperative (Willekens et al. 2003b; Pandey and Rizvi 2010, 2011; Mohanty et al. 2014; Low et al. 1985). But red cells are expensive, i.e., they require significant metabolic effort to produce, and thus, they might well be expected to possess a mechanism to prolong their useful life; *quidem* they possess a self-protective mechanism of vesiculation, i.e., the process of shedding microvesicles that contain degraded molecular species (Willekens et al. 2003a; Ciana et al. 2017a, 2017b; Leal et al. 2018; Bosman et al. 2012). Cells are eventually removed, after sufficient degradation, by processes that fall within the term of cell *clearance* (Safeukui et al. 2012; Groom et al. 2002; Schmidt et al. 1988); this process involves filtering within organs such as the spleen. However, despite the significant role the spleen plays as a "mechanical filter" that role should not be overemphasized in contrast to its overarching lymphatic role in removing unwanted red cells.

A primary mechanism of cell clearance is via sequestration in organs such as the liver and spleen (Willekens et al. 2003a; Ciana et al. 2017a, 2017b; Leal et al. 2018; Asaro et al. 2018; Shah et al. 2018; Allarg et al. 2013) where

✉ R. J. Asaro
Scipio394@gmail.com

[1] Department of Materials Science and Engineering, Massachusetts Institute of Technology, Cambridge, MA 02139, USA

[2] Department of Medical Biophysics, Schulich School of Medicine and Dentistry Western University, London, ON, Canada

[3] Department of Structural Engineering, University of California, San Diego, La Jolla, CA 92093, USA

macrophages live up to their function as *magna comedeni*. This raises the question of how such sequestration comes about. *It is, specifically, by the mechanism of red cell flow through the venous sinus system of the human or rat spleen that we consider herein*; these red cells may pass through the narrow slits of the venous sinus in the red pulp and possibly be induced to vesiculate or become trapped and more readily removed by macrophages. However, they are known to sequester via adhesion within the red pulp en route to the sinuses as well; they may even be induced to undergo hemolysis in the pulp or sinuses as a prelude to clearance by macrophages (Klei et al. 2020). Passage through the IESs may be a vital part of that process.

Senescent cells are marked for removal in various ways as reviewed by Lutz and Bogdanova (2013), see also Willekens et al. (2003b), Pandey and Rizvi (2010), Pandey and Rizvi (2011), Fens et al. (2012). For perspective, it is important to note that a typical red cell may transit the human spleen up to 50–80 times per day during its roughly 120 day lifespan (Asaro et al. 2018); however, not all these passages involve transits through venous slits of the red pulp (Schmidt et al. 1993); depending on the specie of mammal and its health, such fractions lie in the range 10–90% (Cesta 2006). In humans, a red cell undertakes transit via the slow path, i.e., through the red pulp and sinus system in roughly 10% of its splenic passages (Groom et al. 2002). Nonetheless, passage through the *interendothelial slits* (IESs) of the venous sinus is an expected and repetitive event in a cell's lifetime and is a severe test of cell mechanical fitness and viability (Cho and De Bruyn 1975; Pivkin et al. 2016; Li et al. 2018); this process is the central focus of the present study. To analyze cell passage through the IESs, we make detailed use of the unique video microscopy observations of MacDonald et al. (1987), Groom et al. (2002), Schmidt et al. (1988) who hypothesized that, among all factors that may affect IES passage, IES caliber was the prime mediator. We detail these factors below and then present a model for slit caliber and demonstrate its viability via simulation. *The main goals of the analysis presented herein are to first postulate a mechanistic model for the opening of interendothelial slits and then to demonstrate how its various features work to control IES caliber in the manner observed and recorded by* MacDonald et al. (1987), Groom et al. (2002), Schmidt et al. (1988).

With respect to vesiculation, we note the results of Asaro et al. (2018) who have shown analytically, and mechanistically, how vesiculation is promoted by passage of red cells through the splenic IESs and in fact have experimentally demonstrated that when such deformations as occur during slit passage are imposed on blood cells, vesiculation is indeed promoted. *Promoting vesiculation as a self-protective mechanism may, in fact, be one of the more important functions of red cell passage through the IESs.* Slit caliber is an important influence of this process as shown by the results of MacDonald et al. (1987) and Asaro et al. (2020, 2018) and is what motivated the present study. Among the interesting observations of slit caliber described by MacDonald et al. (1987), Groom et al. (2002), Schmidt et al. (1988) are, inter alia, that the multiple slits of a given sinus open and close asynchronously and for relatively brief periods of time ($\sim$ 10s); it is features such as these we attempt to provide a mechanistic explanation for. We also use the analysis to point specifically to required further study to develop a more detailed, predictive, understanding.

Cell adherence to the endothelial cells of the sinus and the fibrous red pulp may play a vital role in cell clearance through the process of red cell lysis as described by Klei et al. (2020), Zimring (2020). Klei et al. (2020) propose that lysis is a precursor to red cell removal by macrophages in that they found that an unexpectedly low percentage of red cells engulfed by macrophages in the human spleen were *intact cells*; the far larger fraction of cells found in macrophages were ghosts, devoid of hemoglobin. Asaro et al. (2020) demonstrated how red cell adhesion, in even modest shear flows, can result in tethering, vesiculation, and evagination and provided a mechanistic explanation of how and why this occurs. Moreover, they found that senescent red cells are far more prone to the loss of membrane and hence to lysis. Indeed, red cell fragments are observed in large numbers as we show below (Fujita 1974) and this points to the role of interendothelial slit (IES) caliber as Asaro et al. (2020) demonstrated—accordingly, the operation of IES caliber is a prime object of the present study. In fact, Klei et al. (2020) stated "However, as erythrocytes within the spleen are forced through endothelial fenestrae to re-enter circulation, we hypothesized that, here, ECM proteins such as laminin-α5 may capture aged erythrocytes." They had said just above that comment "... trapping or retention of erythrocytes under shear forces induces hemolysis." It was precisely this process that Asaro et al. (2020) also hypothesized and analyzed and provides a basis for the current study.

Accordingly, the present study is concerned with how the sinus-IES system behaves and how its active (i.e., not passive) vital features such as slit caliber are established. This detail is required to understand the role of the sinus IESs in processes such as vesiculation and possibly even hemolysis as discussed by Klei et al. (2020).

2 Splenic flow environment: relevant perspectives

The red blood flow environment, essential to our analysis, can be described in Fig. 1a, b taken from Carlson (2018) and Fig. 1c taken from Drenckhahn and Wagner (1986). Figure 1a shows the closed circulation within the spleen where blood flow follows a pressure gradient in endothelial lined

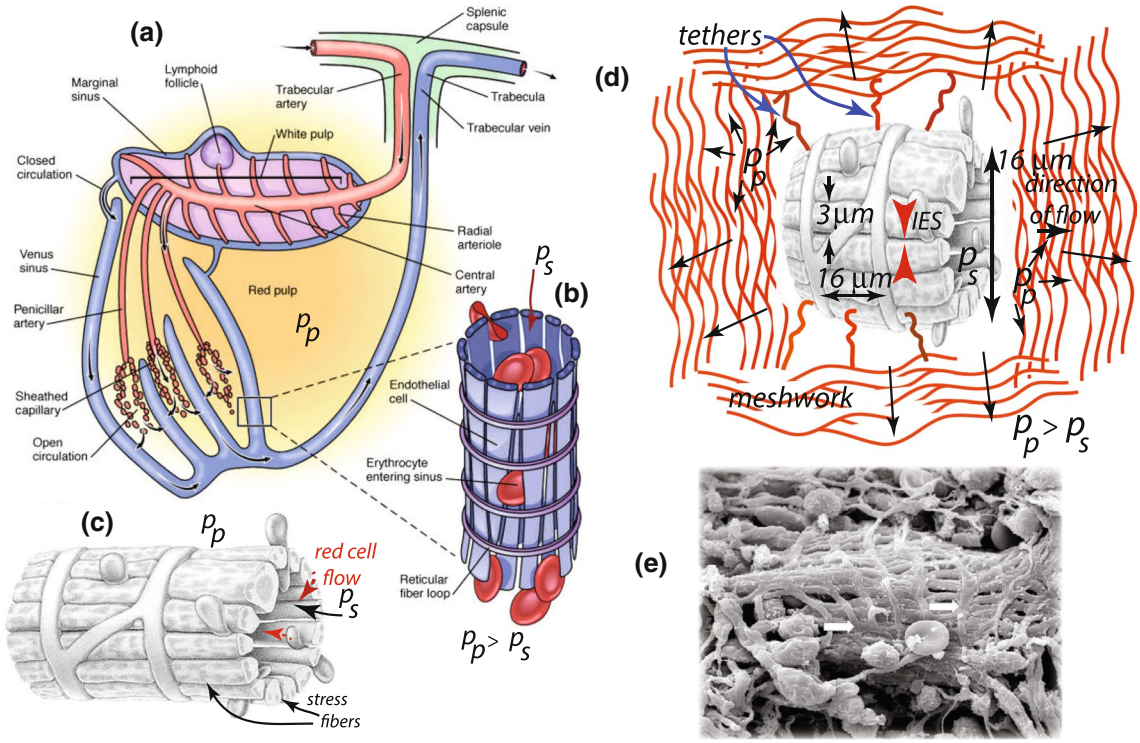

Fig. 1 **a** Microcirculatory flow within the spleen; open flow consists of red cell flow through the reticular meshwork of the red pulp under pressure P_p and possibly through the interendothelial slits (*IES*s) of the venous sinus with interior pressure P_s in the sinus lumen; note $P_p > P_s$ that determines the prevailing direction of red cell flow. **b** Detail of a section of the venous sinus showing long spindle-like endothelial cells (*EC*s) supported by *reticular ring fibers*; note a red cell entering the sinus through an *IES*. **a, b** taken from Carlson (2018). **c** Venous sinus as in (**b**) but showing stress fibers (SFs) running axially along *EC*s; taken from Drenckhahn and Wagner (1986). **d** Depiction of a sinus embedded in a region of red pulp reticular meshwork. Note the porous fibrous nature of the meshwork and its connectivity to the sinus. The "pore pressure" within in meshwork, P_p, expands the sinus due to this connectivity. **e** SEM image of the outer wall of a human splenic sinus, taken from Gálfiová et al. (2009)

vessels from the trabecular artery, radial arteries and marginal sinus to the venous sinuses and trabecular vein leading to the hepatic portal system where the pressure drops to values not greater than ~ 5 mmHg (~ 660 Pa) (Steinger et al. 2011; Zhu et al. 2015; Abraldes et al. 2014). Figure 1a also shows the open circulation where blood from the penicillar arteries empties into the open spaces of the reticular meshwork in the red pulp before entering the venous sinuses via the interendothelial slits (IESs). As flow is from the red pulp into the venous sinuses, the pressure in the red pulp must be greater than in the sinuses, i.e., there must be a negative transmural pressure.

As a negative transmural pressure would normally cause collapse of a vessel, e.g., in the veins of the neck or back of the hand when elevated above the level of the neck, there must be a counteracting outward force acting on the walls of the venous sinuses preventing collapse and closure of the IESs. We propose that fibers of the reticular meshwork in the surrounding red pulp (Blue and Weiss 1981; Thomas 1967; Miyoshi and Fujita 1971), attached to the outer walls of the endothelial cells (ECs) and/or surrounding reticular fiber loops, provide an outward force which prevents collapse of the sinus vessel. Tension in the reticular fibers would be due to eventual attachment of reticular meshwork to the outer capsule of the spleen. Any increase in pulp pressure which would promote collapse of the sinuses would also expand the capsule, increasing tension in the fibers to counteract collapse. On the other hand, the sinuses of fully relaxed spleens in dogs were reported to be often "collapsed" by Blue and Weiss (1981). This observation tends to support our hypothesis. Figure 1b, c depicts a section of the venous sinus, showing red cells passing through (IESs); the frequency of such red cell-slit transit has been described above, and the details of this are described below where the slit width, i.e., caliber, emerges as a mediating factor.

In Fig. 1a and d, we denote the nominal pressure within the red pulp as P_p, while that within the lumen of the sinus by P_s. As $P_p > P_s$, red cells are driven to flow through the IESs into the sinus lumen down a pressure gradient to end in the trabecular vein where they enter the portal; $\Delta P_s = P_p - P_s$ may be referred to as a "driving force"; as noted below, ΔP_s need not be large to drive cells across

an IES as we estimate values to be of $\mathcal{O}(130-200\,\text{Pa})$ as described below. Given the IES caliber, the question arises as to whether a cell can transit an IES and what is the timescale of such transit? IES transit timescale is important since it determines whether red cell skeletal remodeling can occur, i.e., during the observed average 0.1–0.2 s transit times, that allows processes such as vesiculation to occur (Asaro et al. 2018, 2020). Transit times may indeed be much longer and cells may even become adhered to the endothelial slits as the attempt passage into the sinus lumen; some interesting implications of such adherence have been analyzed by Asaro et al. (2020). The video microscopy of MacDonald et al. (1987) is reviewed next as it sheds vital insight into the IES transit process and its kinetics.

Microcirculation through the mammalian spleen is complex and occurs via both "open" and "closed" pathways as already noted; hence, only a subpopulation of blood cells that transit through the spleen pass through venous slits. For example, as noted by Schmidt et al. (1988), "major routes for entry of blood into venous sinuses appears to be via open ends in continuity with the MZ (i.e., the marginal zone)"; this route bypasses the IESs. Alternatively, MacDonald et al. (1991) have found that open circulation is via the penicillar arteries which dump into the reticular meshwork of the red pulp. Here, the RBCs percolate through to the venous sinuses interacting with their surroundings before re-entering the circulation. Because these interactions cause them to move slower than the plasma, the hematocrit increases (MacDonald et al. 1991). Once inside the reticular meshwork of the red pulp, cells exist in a crowded environment and interact via direct contact with other cells before entering the venous sinuses. Hence, cells are not free flowing individuals as visualized in simulations such as shown in Fig. 2a; these simulations (Asaro et al. 2020) are discussed below. The effects of such direct contact interaction on either deformations, transit timescales, or orientation are as yet to be determined.

Also relevant is that the crowded venous environment, as just noted, is characterized by a high hematocrit which in dogs, for example, may be as high as 90% (Opdyke 1993; Opdyke and Apostolico 1966) and as high as 79% in cats (Levesque and Groom 1976); in such mammals, as dogs or horses up to 50% of the body's RBCs may be sequestered in the spleen at rest where this results in reduced blood viscosity in the vasculature and hence reduced demands on the heart. In humans, however, the splenic hematocrit is much lower, which motivates the view of the human spleen as a lymphoid organ. Nonetheless, MacDonald et al. (1991) have estimated that hematocrit may be as high as 78% in the human spleen and this motivates our choice of viscosity

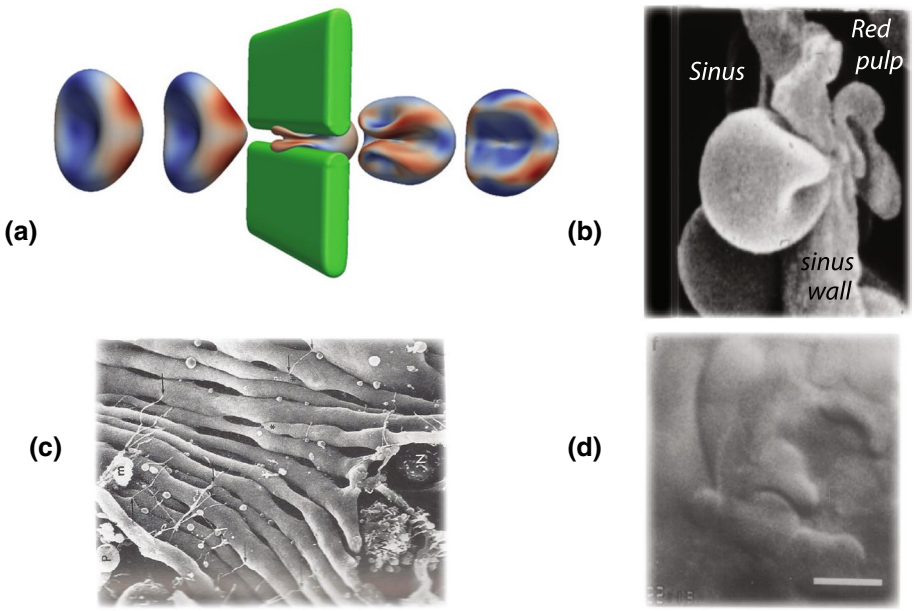

Fig. 2 **a** Influence of RBC initial orientation upon entering a venous splenic slit on the cell's deformation shape; in this orientation, the cell undergoes large deformations and develops an in-folded region upon exiting the slit (taken from Asaro et al. 2020). The width of the slit in (**a**) was 1 μm. Note the *in-folded* region of the cell that has been forecasted (Asaro and Zhu 2020) leads to extreme stresses that tend to separate the skeleton from the membrane. **b** Red cell passing through an IES, taken from Biosfleury and Mohandas (1977) or Mohandas and Gallagher (2008); note the in-folded region as in (**a**). **c** Endothelial cells of the venous sinus as taken from Fujita (1974). Note the parallel, rod-like, morphology of the endothelial cells and also the slit just upper right of a cell fragment marked "E"—this slit as is has dimensions $\sim 7.5\,\mu$m in length and a caliber of $\sim 0.81\,\mu$m. **d** A red blood cell adhered to the endothelial cells of an IES in a rat spleen; the cell's main body lies within the lumen of the sinus (taken from MacDonald et al. 1987)

in the simulations described by Asaro et al. (2020). This also suggests that the splenic red pulp medium viscosity is rather high, perhaps on par with the RBC cytosol viscosity, which has direct implications for RBC rheology and deformations along with the internal membrane-skeleton forces generated by deformations. We note additionally that as red cells flow through the reticular meshwork of the red pulp they are retained, i.e., sequestered, by adherence to the meshwork (Song and Groom 1971, 1972, 1974) where they may be removed; since the interstices of the meshwork are larger than red cells, such passage does not constitute a test of cell *deformability*. This may point to the realization that red blood cells may be removed for a variety of reasons that indeed pertain to their deformability (Diez-Silva et al. 2010, 2012; Safeukui et al. 2018; Henry et al. 2020) but also to other characteristics such surface characteristics as affected by aging and/or diseased states (Groom et al. 2002; Wautier and Wautier 2013; Wautier et al. 1981, 1994; Pernow et al. 2019; Wautier et al. 2011; Bonomini et al. 2002; Closse et al. 1999; Henry et al. 2020).

3 Kinetics and flow patterns of IES transit by red blood cells

3.1 Basic features of red cell transit

Essential features of red cell transiting IESs are addressed, in brief, in Fig. 2a, b, whereas Fig. 2c provides perspective, via a SEM micrograph, of the long spindle-like ECs of the, in this case, rat sinus wall; the gaps between the ECs, although distorted by freeze drying, are visible—these are the IESs, as discussed below.

Figure 2a, taken from a simulation of Asaro et al. (2020), is a snapshot of a red cell, with an initial orientation as shown at the left, approaching and passing through a slit of caliber $\delta = 1\,\mu$m; this cell was "driven" by a pressure difference of 200Pa ($\sim$ 1.5 mmHg) across the slit, i.e., we set $\Delta P_s = 200$Pa in the simulation. As we will see below, and consistent with this, we estimate the pressure differential across an IES, i.e., $\Delta P_s = P_p - P_s$, to be of $\mathcal{O}(130-200\,\text{Pa})$ in our model of the IES caliber. Figure 2b, taken from Biosfleury and Mohandas (1977), shows a red cell emerging after transiting an IES where we note that the in-folded region provides for the veracity of such simulations. Given the fidelity of our simulations to such observations, we find it compelling to also hypothesize further that slit caliber is a primary mediator of red cell IES passage as has been demonstrated by earlier studies, e.g., Pivkin et al. (2016), Zhu et al. (2017), Asaro et al. (2018), Li et al. (2018), Asaro et al. (2020). Figure 2d is discussed next where we review the truly compelling evidence for slit mediation based on the video microscopy of MacDonald et al. (1987).

Figure 2c (from Fujita 1974) shows a SEM images of the sinus interior and wall of a human spleen. Fujita (1974) describes the endothelial cell walls as "rods" with "slits" separating them, although care must be taken in any literal interpretation of slit character as seen in such images due to methods employed that included the fixing of organs and quench-freezing in liquid nitrogen. Hence, although care was taken to preserve structure by fixing, attempts at establishing precise dimensions from such snapshots require scrutiny. Moreover, and crucially, there is no understanding of what physiological processes were in place, in vivo, when such "openings" as shown in Fig. 2c were formed. With these caveats, though, we notice that the size scale of such slit-like openings are of $\mathcal{O}(\sim 6-8\,\mu\text{m})$ in length, with an average of $\sim 7.0\mu$m, with calibers of $\mathcal{O}(\sim 0.5-1.0\,\mu\text{m})$; smaller openings may possibly be viewed as *nascent slits*, with again the above caveats and cautions. If a larger set of the SEM images of Fujita (1974) are used to estimate sinus diameter they yield, again with a rather wide and approximate range, 10−16 μm, with an average of $\sim$ 13 μm. Likewise, the range of EC diameters would be in the range 2.0−2.7 μm, with an average $\sim$ 2.35 μm; we note that these values could be adjusted upward to account for small amounts of shrinkage that occurs during freeze drying. These values are summarized in Table 1 where we use them to define a *working structural sinus model* (WSM). We note as well that the size range of sinus slits used in various analysis of sinus-slit passage have used slit calibers that incorporate this size range, e.g., as in Asaro et al. (2020), Asaro et al. (2018), Zhu et al. (2017), and hence, this provides veracity of those choices. We note, however, other uncertainties such as whether or not ring fibers visible in the existing various images of the sinus wall actually form continuous hoops that constrain ECs as hoops of a barrel or are lengths of fibers that just connect continuous hoop fibers. This is a feature of the schema shown in Drenckhahn and Wagner's Fig. 1c and suggested in Fig. 1e taken from Gálfiová et al. (2009). Drenckhahn and Wagner (1986) report spacings, based on optical microscopy, of individual ring fibers in the human spleen in the range 4−5 μm (see their Fig. 9a, b) but again whether all these individual fibers form continuous hoops is unclear. With such interpretations, the length of ECs along slits would be judged to be somewhat larger than estimated above. With the provisos of above, we believe that the images of Fujita (1974), such as shown in Fig. 2c, do provide veracity to the model depictions described below.

We add a specific note that Chen and Weiss (1972) had concluded, from their electron microcopy of the human spleen, that "The endothelium (of the human venous sinus) is held together primarily by the ring component of the basement membrane (the ring fibers)...". In the context of our model for the sinus, this implies that if the ring fibers expand, the sinus diameter expands, and hence, the IES

caliber increases as endothelial cells separate further with the expanded sinus perimeter. This is noted below in the analysis of our simulations of caliber development.

It is noted that the rat is the most commonly used experimental animal with a spleen anatomically similar to the human's (Groom et al. 2002). Rats, dogs, and humans have sinusoidal spleens, whereas cats, mice, horses, pigs, and cows have non-sinusoidal spleens. Rats and humans also have both open circulation (through the reticular meshwork), as noted herein, and closed circulation (by direct connection of arterial capillaries to venous sinuses). The dimensions of slit caliber and red cell dimensions in humans and rats are, coincidentally, in rough proportions, with those of the rat being about 15–19% less. Hence, computational models are essentially scaled accordingly from one specie to the other and indeed provide consistent patterns of deformation and response.

3.2 Kinetics of erythrocyte splenic IES transit

The picture we have, then, is one in which cells are driven through the reticular meshwork, and thereby through venous slits, by an imposed fluid shear flow, or its compliment an imposed pressure differential, that varies with time with frequencies of $\mathcal{O}(0.1–0.2$ Hz) as sketched, perhaps, in Fig. 3b. For reference, the transit times for cell passage through slits (in rat spleens) reported by MacDonald et al. (1987) were of $\mathcal{O}(10^{-2}$ s-2×10^{2} s) with quite skewed distributions with medians of $\mathcal{O}(2 \times 10^{-1}$ s) and means of $\mathcal{O}(2$ s). These timescales are indeed quite disparate, varying by factors of 10, respectively, yet we must look more deeply into the behavior of the slit caliber before a sufficient picture becomes clear.

Next, we recall the MacDonald et al. (1987) hypothesis that the variations in venous slit caliber were "primarily responsible for the observed patterns of (cell) flow." Moreover, they reported that "bursts" of flow through two closely spaced slits were asynchronous; hence, the slits operated somewhat independent of each other; that is, their caliber was not strictly mediated by the prevailing "driving force" at a particular time; likewise, cell passage through nearby slits was not evidently correlated with patterns, or rates of, or pressure within, blood flow within the lumen upon exist. In fact, since the bursts in adjacent slits were asynchronous, they did not appear to be strictly mediated by patterns of pressure in the red pulp's reticular meshwork as the pattern for P_p in Fig. 3b may perhaps describe. These bursts of cell passage would appear to have durations of $\sim \mathcal{O}(10$s) as judged, e.g., by examination of MacDonald et al.'s Fig. 4 (MacDonald et al. 1987), and this would set an important timescale for cell-split passage. On the other hand, slit caliber would also be mediated, it appears, by the contractility of the stress fibers discussed above in connection with Figs. 1c or 3a. Induction of stress fibers in human endothelial cells, in turn, may be triggered by ATP (Drenckhahn and Wagner 1986) or shear force imposed via fluid flow (Franke et al. 1984). Franke et al. (1984) demonstrated stress fiber induction under shear stresses of $\mathcal{O}(\sim 0.2$ Pa), and Drenckhahn and Wagner (1986) showed that contractility was induced in human splenic endothelial cells with the use of *Mg*ATP; in the latter case, induction was induced after periods of time of $\mathcal{O}(1–2$ min); but this, of course, does not

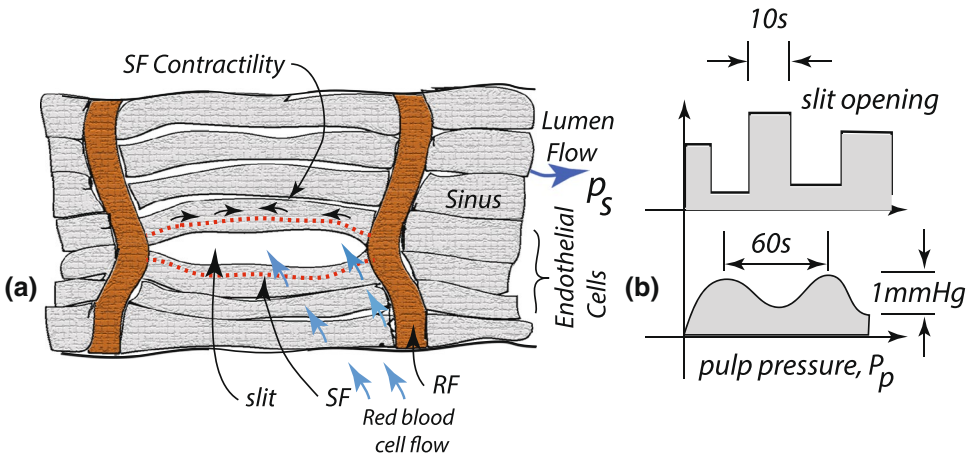

Fig. 3 **a** Possible mechanism of stress fiber contractility inducing the opening of a venous slit. Note that such a mechanism may also suggest that next-neighbor slits may be closed, unless the endothelial cells (ECs) develop a double curvature, in which case slits may be opened on either side of a given EC. Note that a slit opening responds to a RBC attempting to transit the imminent slit opening between endothelial cells. Slit width would be set by the spacing of the "annular," or "ring," fibers (Chen and Weiss 1973; Mebius and Kraal 2005) which is about 1–2 μm in the rat spleen, and probably larger in the human venous sinus. **b** Schematic of pressure P_p, at bottom, in the reticular meshwork of the red pulp which represents a driving force for red cell entry into the sinus lumen through the venous slits and, in the upper sketch, a possible time sequence of IES caliber versus time as observed by MacDonald et al. (1987)

set any characteristic timescale for the long-time, ongoing, conditions prevailing within the red pulp. Taken together, a temporal scenario of "driving force"—be it pressure differential or imposed blood flow—and slit caliber might look something like that sketched in Fig. 3b. Note that before considering this further several points require consideration.

It is also interesting to note that Chen and Weiss (1973) reported that "There are no preformed apertures in the (splenic) sinus walls. Instead, slits between the sinus endothelial cells, which are otherwise closed, are widened while cells pass through them." They went on to say "The slits are closed except when penetrated by blood cells, platelets, or macrophages." (Chen and Weiss 1973); similar conclusions were arrived at by Cho and De Bruyn (1975) regarding the absence of preformed slits of finite caliber. Of course, to approach the sinus wall the red blood cells would have to be carried by movement of plasma either through narrow slits or along the sinus wall. To allow for continuous blood flow, it may be that at any given time various slits may open and others close. Nonetheless, it appears that the sinus endothelium "responds" to contact with RBCs by opening slits to some caliber appropriate to allow them passage. What triggers this, is as yet, unknown but may be release of ATP by RBCs attempting to transit the sinus wall. A possible mechanism is sketched in Fig. 3a involving the activation of contraction of stress fibers which is known to be ATP dependent (Drenckhahn and Wagner 1986). We add an, albeit anecdotal, observation of Thomas (1967) that in the sinusoidal spleen of dogs, IESs are found to be open even without evidence for RBCs to be passing; our paradigm is consistent with this possibility.

Here, we note that contractility of stress fibers can cause an opening of a slit between endothelial cells whose caliber may be, accordingly, set by the spacings between the annular, or ring, fibers as noted by Mebius and Kraal (2005), Drenckhahn and Wagner (1986), or Chen and Weiss (1973); for example, this width would be of $\mathcal{O}(1-2\,\mu m)$ in the sinus of the rat spleen as noted by Chen and Weiss (1973). According to this hypothetical scenario, slit openings depend on asymmetrical contraction of stress fibers within a given endothelial cell. The asymmetrical contraction of stress fibers suggested here may also have been observed in the asymmetrical contractions seen during the spontaneous contraction of capillary walls in vivo within the rat spleen by Ragan et al. (1988). More generally, the role of stress fiber contractility in vascular endothelial cell contraction has been well documented (Shen et al. 2009; Essler et al. 1999; Bauer et al. 2000).

Although the conceptual model just outlined may explain the asynchronous opening of "adjacent slits," it may not fully explain the degree to which they open; for this may be needed a more general picture of opening slits and one that does not depend on the asymmetry of stress fiber activation. We thereby also propose that since the sinus is attached to the reticular meshwork and that even though its pressure is such that $P_p > P_s$, increases in P_p may, in fact, cause the sinus to "follow" the red pulp's expansion which would lead to a general swelling of the sinus and opening of its IESs. Moreover, if some ECs are contracted with time, symmetrically or not, the stiffening of ECs will lead to asymmetrically opening of IESs. Our full model of the sinus, considered next, presents this more general scenario, followed by simulations that reveal the sinus and IES response. Hence, we first hypothesize that a more holistic view of the pressure field inside the region surrounding the red pulp and the sinus may be required, especially in how it may transmit forces on the sinus, as well as attention paid to the response of individual endothelial cells that comprise the sinus wall.

3.3 Splenic pressure distribution and endothelial contractility

We next hypothesize that pressure acting at the capsule wall of the spleen, herein dubbed the *capsulic pressure*, P_c, transmits forces acting within the red pulp that, in turn, impose forces that act to expand the sinus; these forces thereby support opening of the sinus. As the capsule is not spherical yet stiff, any increase in P_c will increase the volume of the spleen and thus tension the reticular fibers within it that connect the sinus and capsule walls. These forces thereby support opening of the sinus; these forces are accounted for by an outward pressure called P_{pull} described below. Moreover, the known contractility of the stress fibers will affect slit caliber in at least two essential ways; these are: (1) a symmetrical stiffening of individual endothelial cells caused by stress fiber contraction and (2) an asymmetrical contraction of stress fibers in individual endothelial cells that may cause additional slit opening due to EC bending as sketched in Fig. 3a. Note that within a given sinus adjacent slits will open in an uncorrelated fashion via these mechanisms, whereas simple mediation of the pulp pressure P_p would induce a more axisymmetric response.

To explain the specific model that we describe in detail, and analyze, below we first discuss the overall pressure field within the spleen as it may affect the forces acting on the sinus. This is done using a simple model we dub the *cylindrical spleen model*, sketched in Fig. 4.

The sketch illustrates arterial blood flow entry into the marginal zone of the spleen below the capsule, where arterial resistance R_a occurs. From there blood takes one three routes where we are focused on the open path through the red pulp where eventually entry into the sinuses via the IESs occurs; we recall that this pathway accounts for about 10% of the total splenic blood flow. In the red pulp the pressure drops to P_p as it approaches the sinuses, where red cells are driven through the IESs into the sinus lumen under driving

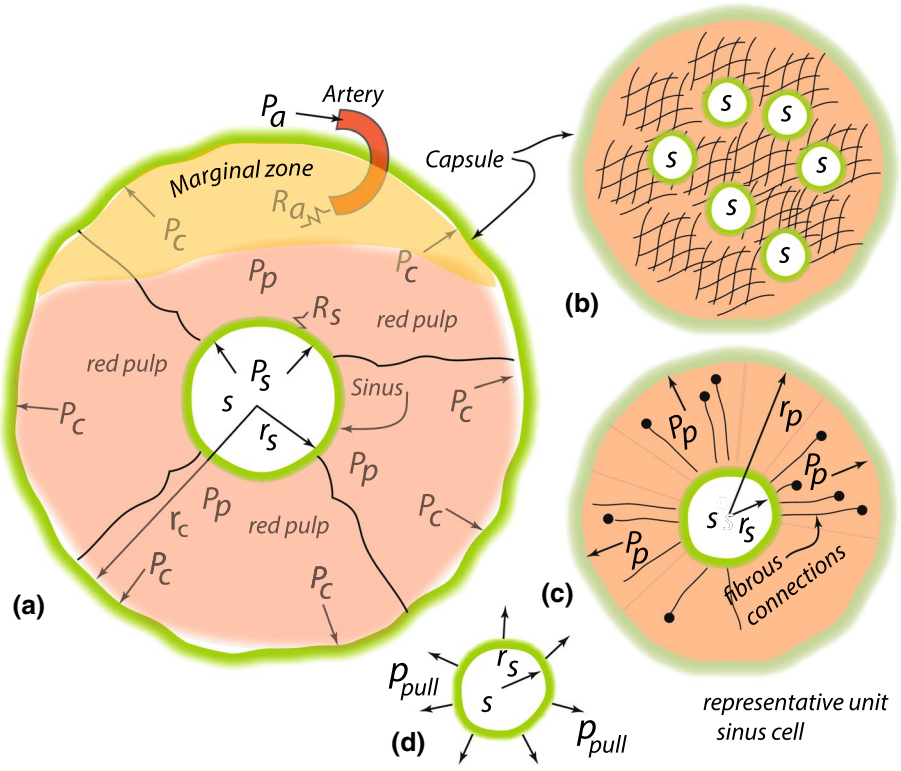

Fig. 4 **a** Cylindrical model of the spleen, indicating a sinus with internal pressure P_s and red pulp under pressure P_p and the capsule wall under pressure P_c. **b** Indicates multiple sinuses that en toto have a net surface area on the order one half that of the capsule wall. **c** A conceptual model within the cylindrical spleen model that depicts a representative sinus unit cell subject to a force imparted to it by pressure of the surrounding pulp of radius r_p; the radius of the sinus is r_s. **d** a conceptualization of the outward effective forces, viewed as a pressure P_{pull}, expanding the sinus

force ΔP_s with resistance R_s. Hence, the kinetic path is, albeit greatly simplified, given as

$$P_a \overset{R_a}{\rightsquigarrow} P_p \overset{R_s}{\rightsquigarrow} P_s, \tag{1}$$

with the fluxes being assumed linear as

$$\begin{aligned} &j_i = \frac{1}{R_i}\,\Delta P_i, \quad i = c, s, \quad \text{with} \\ &\Delta P_C = P_a - P_p, \quad \Delta P_s = P_p - P_s. \end{aligned} \tag{2}$$

The flux resistance constants, R_i, are described by Groom et al. (2002). In using a simple flux balance we take into account the multiple sinuses, as depicted in Fig. 4a, whose total peripheral area compare with that of the capsule wall; hence Eqs. 1–2 are effectively the results of a mass balance. If we assume a steady flow, i.e., j_i = constant, we arrive at

$$P_p = \frac{P_a - P_s}{(R_a + R_s)/R_s} + P_s. \tag{3}$$

To gain some perspective on the numerology, we take $P_s \sim \mathcal{O}(10\,\text{mmHg}) \sim \mathcal{O}(1.33\,\text{kPa})$, $R_a = 89$, $R_s = 1$, and $P_a = 100\,\text{mmHg} = 13.3\,\text{kPa}$ (Groom et al. 2002; Atkinson and Sherlock 1954). With such numbers, we obtain $P_p \approx 11\,\text{mmHg} \approx 1.46\,\text{kPa}$. This is slightly larger than the range we have previously used in our simulations of red cell flow through the IES system. An example of such simulated results is shown in Fig. 2a; in those simulations $\Delta P_s = 0.2k\,\text{Pa}$ (Asaro et al. 2020). On the other hand, if we had taken $R_A \sim 50$, Eq. 2 would yield $P_p \approx 11.76\,\text{mmHg} \approx 1.55\,\text{kPa}$. In this way, we arrive at the tentative range $200\,\text{Pa} \le \Delta P_s \le 234\,\text{Pa}$. We note that the sinus pressure of $P_s = 10\,\text{mmHg}$ has been assumed in these estimates since we expect the downstream portal pressure to be closer to the range near 5 mmHg in healthy humans (Steinger et al. 2011; Zhu et al. 2015; Abraldes et al. 2014). However, it is possible for the lumen pressure to be somewhat higher or for the red pulp pressure somewhat lower so that ΔP_s falls to values of order $\Delta P_s \sim 0.5\,\text{mmHg}$ (66.7 Pa), yet we always realize that $P_p > P_s$.

With the above numerology, we arrive at an estimate for P_p that lies within the range $11\,\text{mmHg}\,(1.46\,\text{kPa}) \le P_p \le 12\,\text{mmHg}\,(1.6\,\text{kPa})$. We note that P_p exerts an outward pressure on the splenic capsule wall that exerts opening forces on the sinuses that are tethered to it via the reticular meshwork of the red pulp; this is indicated in Fig. 4a. This pressure applies opening forces on the sinuses due to connectivity of the red pulp meshwork to the endothelial cells of the sinus. It is because of this tethering that the sinus may be expanded despite the fact that $P_p > P_s$. To estimate these forces, we appeal to Fig. 4b-c and model the sinus of radius r_s, i.e., within our *cylindrical spleen model*, to be encapsulated within meshwork of radius r_p. In a "rest" state, we take $P_p \ge P_s \approx 10\,\text{mmHg}$ and hence the additional expansion of the sinus is due to the excess pressure

$\Delta P_s = P_p - P_s \approx 1$ mmHg; we may readily imagine that ΔP_s may lie in a range of, say, $0.25\,\text{mmHg} \le \Delta P_s \le 1.0\,\text{mmHg}$ and if we assume that $r_p \sim 2{-}3r_s$ we have a net outward pressure, we call $P_{\text{pull}} = (r_p/r_s)\Delta P_s$, in the range $0.5\,\text{mmHg} \le P_{\text{pull}} \le 3\,\text{mmHg}$. In our simulations, presented below, we explore the range $0.5\,\text{mmHg} \le P_{\text{pull}} \le 3\,\text{mmHg}$ as this range, indeed, produces IES openings of physiological relevance. Taking $r_p \sim 2{-}3r_s$ is justified be estimating the area fraction of sinus within the context of the cylindrical spleen model.

It is important to note that the pulp pressure applies the pressure P_{pull} via the tethering of the reticular meshwork to the sinuses. Hence, we effectively apply a force, as a pressure P_{pull}, and not a displacement; the displacement at r_p, or for that matter at the capsule wall, does not enter the analysis of the sinus expansion. A simulation of the entire splenic volume would, in principle, allow an estimate of the expansion of the capsule wall. This is, however, not our objective here. More notes and discussions can be found in the Discussion section.

The connectivity of the splenic reticular meshwork to endothelial cells and, in particular, to the splenic sinuses in rats has been described in some detail by Saito et al. (1988). They describe such detail as the connection involving the "... basement membranes of the sinuses being sandwiched between reticular cells and sinus endothelial cells." They go on to propose that the meshwork not only supports the spleen but "... also contributes to a contractile mechanism in circulation regulation"; this involving contractile fibers. We do not, however, interpret their phrase *contractile mechanism* to suggest that the rat spleen, or the human spleen, is overall contractile; it is the connectivity that is most relevant. Hence our paradigm fits generally within this picture and is supported by the observations of Sato et al. (2001). We have simplified the structure of this connectivity by referring to "tethering" where the mechanical functionality is equivalent.

We explore an additional feature in our model, viz. that of the contractility of the stress fibers (SFs) as sketched in Fig. 3a. On the one hand, the fibers of a given endothelial cell (EC) may symmetrically contract which leads to a stiffening of the cell in bending. On the other hand, an asymmetrical SF contraction would induce a buckling-like bending of an EC that further opens an adjacent slit. Note that whereas unsymmetrical SF contraction would lead to an opening of only specific slits of the sinus, so would symmetrical SF contraction if adjacent slits are affected differently, e.g., stochastically. Hence the action of SF contractility would lead to an asynchronous slit caliber activity as emphasized in the results of MacDonald et al. (1987) and also discussed by Groom et al. (2002). Taken together, these two elements of our model, viz. capsulic pressure and EC stress fiber contractility, serve to induce a transient slit opening that is asynchronous among the slits of a given sinus.

3.4 An elastic analog model

To put the basic ideas into a finer focus, we consider Fig. 4c and view the sinus conceptually, as a cylindrical cavity in a linear elastic medium, viz. the reticular meshwork, subject to a outer boundary outward pointing pressure, P_c. The sinus has radius r_s, and the outer capsule boundary has radius r_c. Since the interior of the sinus is a fluid with a pressure, P_s nearly equal to the red pulp pressure, P_p we take the sinus to be a "cylindrical hole"; this is depicted in Fig. 4c. We note, however, that this conceptual model shall be replaced by a far more detailed structural model for the sinus just below.

The solution for the radially symmetric displacement, $u_r(r)$, to this problem is well known (Asaro and Lubarda 2006; Sadd 2005) and is given

$$u_r(r) = \frac{1+\nu}{E}\, r\Big\{(1-2\nu)B - \frac{A}{r^2}\Big\}$$
$$A = -\frac{r_s^2 r_c^2 P_c}{r_c^2 - r_s^2}, \quad B = -\frac{r_c^2 P_c}{r_c^2 - r_s^2}. \tag{4}$$

Now, for our reticular meshwork we take Poisson's ratio as $\nu \approx 0.5$ simulating an incompressible medium containing viscous fluid and a high red cell hematocrit. Moreover, for the purpose of estimates on displacement magnitudes we take $r_c \gg r_s$ so that Eq. 4 becomes

$$u_r(r) \approx \frac{3}{2}\,\frac{r_s^2}{r}\,\frac{P_c}{E}. \tag{5}$$

As approximate as this may be, it does allow for a conceptually useful understanding.

With $P_c \sim 12\,\text{mmHg} \approx 1.596\,\text{kPa}$ and $E = 10\,\text{kPa}$ we find at the sinus periphery, $r = r_s$, $u_r(r_s) \approx 0.225 r_s$. On the other hand at the far field, e.g., at $r = r_c$, u_r falls to quite low magnitudes since we must now interpret r_c as much larger than simply $5r_s$. What this means is that we expect the sinus periphery to expand by about $2\pi u_r(r_s)$ and if $r_s \sim 7{-}8\,\mu\text{m}$ this means the periphery expands on the $\mathcal{O}(1.4r_s \sim 10.5{-}11.2\,\mu\text{m})$.

As just noted, by assuming the red pulp constitutes a nearly incompressible medium we find quite small expansion at $r = r_c$. Yet if $\nu \neq 1/2$ the results is different due to the term involving B in eq. 4. That term would add a contribution to u_r of

$$(1-2\nu)\frac{3}{2}\,\frac{P_c}{E}\,r \tag{6}$$

which has a very different behavior as a function of r. But the assumption of near incompressibility appears sound for now. Hence we expect that the effects we envision would involve substantial expansion of the sinuses with quite modest expansion of the red pulp itself. We use this simple

elastic model below to estimate opening of the sinus due to expansion of the ring fibers.

We now present the more detailed structural model of the sinus, mentioned above, and the loading applied to it, and the simulation goals and expectations.

4 Slit Caliber model and simulation goals and expectations

We have developed a finite element structural model for the splenic sinus that provides for the veracity of our paradigm. The structural model is patterned closely after the microscopic images described above and, for example, as summarized by Groom et al. (2002). In this, we have incorporated several levels of detail in terms of boundary conditions imposed on the endothelial cells (ECs) of the sinus, e.g., as to whether their ends are fixed, with and without uniform stress fiber contraction (our Model 1); or with nonuniform stress fiber contraction and where the EC ends are allowed to rotate (our Model 2). Accounting for the contractility of the stress fibers causes a stiffening of ECs and if their contraction is asymmetric causes EC bending; both effects affect IES caliber. We again note that these contractility effects can account for the asynchronous action of the IESs of a given sinus, and indeed of even slits that are "nearest neighbors" in a given sinus, as observed by MacDonald et al. (1987), Groom et al. (2002).

Our approach to describe the development of IES caliber is designed for clarity in that we first describe the essentially axisymmetric expansion of the sinus, and thereby the IES calibers, under the action of the all-around pressure P_{pull} and then add the more complex effects of the process involving EC bending, that may be asymmetric due to the contractility of the stress fibers; the latter analysis is based on a numerically based finite element model and simulations. IES opening due to axisymmetric the all-around opening pressure P_{pull} is called δ_s^0 and that due to EC bending δ_s^b; hence the total caliber is $\delta_s = \delta_s^0 + \delta_s^b$.

4.1 Axisymmetric expansion of the sinus

The above solution given by Eqs. 4 may be used to estimate the general expansion of the ring fibers and thereby the sinus under the pulling pressure P_{pull}. For this we again take $\nu = 0.5$ and obtain

$$u_r = \delta r_s^0 \approx \frac{3}{2E}\,\frac{1}{r_s}\,\frac{r_{so}^2 r_{si}^2}{r_{so}^2 - r_{si}^2}\,P_{\text{pull}} \tag{7}$$

where r_{so} and r_{si} are the outer and inner radii of the ring fibers; note that r_s would be taken as $r_s = 1/2(r_{so} + r_{si})$. Note that u_r has the interpretation of an increase in r_s and hence the δr_s^0 symbolism. We let $r_{so} = r_{si} + t$ where t is the ring fiber thickness, assumed such that $t \ll r_s$; this approximation accounts for the approximation in eq. 7. We then take $t = 3\mu$m for an estimate and arrive at the result

$$\delta r_s^0 \approx \frac{3}{4}\,\frac{r_s}{t}\,\frac{P_{\text{pull}}}{E}\,r_s. \tag{8}$$

To obtain an estimate for the change, i.e., increase, in slit caliber we take $P_{\text{pull}} = 200\,\text{Pa} \approx 1.5\,\text{mmHg}$ and $E = 10\,\text{kPa}$ and $r_s = 8\mu$m and find that $\delta r_s^0 \approx 1.28\mu$m and hence the average of 12 slits has an expected increased caliber of $\delta_s^0 = 2\pi\delta r_s/12 \approx 0.67\mu$m. To this axisymmetric expansion, we will add the additional displacements that arise due to EC, potentially asymmetric, bending where we fix the ring fibers positions in their axisymmetric locations.

4.2 Asymmetric sinus model and applied forces

The basic model is shown in Fig. 5, whereas details are as follows.

Model and simulation details:

1. *Working sinus structural model (WSM)* Although the essential structure of the venous sinus is clear, detailed dimensions are difficult to specify as we have noted above. We have therefore formulated a working structural model (WSM) that captures the essential features and is adjustable to accommodate dimensional sensitivity studies. We later adjust this model taking into account a broader range of imaging data on human splenic sinuses. The primary WSM is based on what appeared to us to be the most reliable dimension, viz. that of the sinus diameter, D_S; we take this to be $\sim 15\,\mu$m as listed in Table 1. We then use the conceptual schemas of Drenckhahn and Wagner (1986) and/or Mebius and Kraal (2005) and take EC length and diameter to

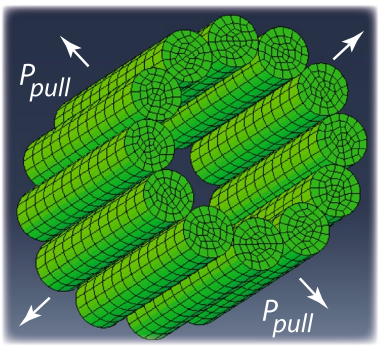

Fig. 5 FEM model of the sinus that resembles a barrel with 12 endothelial cell slats; constraints by ring cells are modeled by boundary conditions described in the text. Note that the sinus opens under the action of the outward pressure P_{pull} as described in the text

Table 1 Key parameters in the analysis for vesiculation due to RBC-EC adhesion in spleen and values considered for the working sinus structural model (WSM)

Expected caliber of inter-EC slits	$\mathcal{O}(\sim 1-1.5\,\mu m)$ (Mebius and Kraal 2005; MacDonald et al. 1987)
Hematocrit in human spleen	as high as 78% (MacDonald et al. 1991)
Young's modulus endothelial cells (ECs)	2–14 kPa (Sato et al. 2001; Kang et al. 2008; Kataoka et al. 2008)
Pressure within sinus, P_s	1.33 kPa (10 mmHg) see text
Pressure within red pulp, P_p	1.46 kPa (11 mmHg) see text
Pulling pressure, P_{pull}	66.7–400 Pa (0.5–3 mmHg) see text
Sinus structural properties	
Sinus diameter (D_S)	12–20 µm (Fujita 1974)
EC cross section diameter (D_{EC})	2.0–2.7 µm (Fujita 1974)
IES width (W_{IES}), EC length (L_{EC})	6–15 µm (Fujita 1974)
Working Structural Model	
D_S, D_{EC}, W_{IES} (aka L_{EC})	15 μm, 3 μm, 8 or 16 μm, see text

be $L_{EC} = 8-16\,\mu m$ and $D_{EC} = 3\,\mu m$, respectively. We note that as the primary deformation mode is bending and that since the maximum bending deflection would scale as L_{EC}^3/D_{EC}^4, the expected EC deflections would be comparable to those with the somewhat uncertain "averages" of $\bar{L}_{EC} \sim 9\mu m$ and $\bar{D}_{EC} \sim 1.8-2\,\mu m$. We also note the sinus image of Gálfiová et al. (2009) in Fig. 1e that suggested that the EC length may be larger than the erstwhile estimated average of $9\mu m$. The WSM, accordingly, has 12 ECs arranged around the sinus perimeter with the above dimensions as listed in Table 1. With these considerations, we later perform the bulk of our simulations using $L_{EC} = 8\,\mu m$.

2. *Constraints by ring cells* The effective constraints provided by ring cells were modeled by boundary conditions described below. The boundary conditions define two basic models called Model 1 and 2 as noted above and explained below.
3. The FEM sinus section model was set up using a commercial package Abaqus (Dassault Systémes Simulia Corp., Providence, RI, USA). Quadratic, reduced-integration (C3D20R) elements were used. Contacts between adjacent ECs were also modeled wherever applicable.
4. ECs were modeled as linear elastic with a Young's modulus of in the range $2.5\,kPa \le E \le 10\,kPa$ and a nearly incompressible value for Poisson's ratio of $\nu = 0.45$.
5. The pressure internal to the sinus was taken as $P_s = 1.33\,kPa \approx 10\,mmHg$ and outside $P_p = 1.46\,kPa \approx 11\,mmHg$.
6. The effective puling pressure to the sinus was taken as $P_{\text{pull}} = 66.7-400\,Pa$ (0.5–3 mmHg).

4.3 Boundary conditions on EC ends: ring fibers

Various boundary conditions were used to simulate the section of sinus modeled here; the section of sinus considered lies between two ring fibers that form complete hoops as discussed above. Results for three such models are presented here.

1. *Model 1:* In model 1, the ECs are fixed so that their end-to-end lengths are held constant; likewise, their ends are prevented from rotating. This is a highly constrained configuration that is relaxed in Model 2.
2. *Model 1a:* In Model 1a, we allow uniform stress fiber contraction as illustrated in Fig. 6a. Stress fiber contraction stiffens the ECs as the results will demonstrate. However, as the schema of Fig. 3a suggests, the ring fibers are quite flexible in bending and allow the EC ends to rotate. Moreover, as the section of sinus we simulate is connected to what in comparison is a very long flexible tube-like structure, the end-to-end distance of the ECs may change with only modest resistance; we take this to allow for the small displacements due to the rotations at the ends of the ECs. The magnitudes of the contractions we impose are consistent with those reported by, e.g. Drenckhahn and Wagner (1986), Franke et al. (1984) and Nehls and Drenckhahn (1991), as listed in the tables below for various model studies.

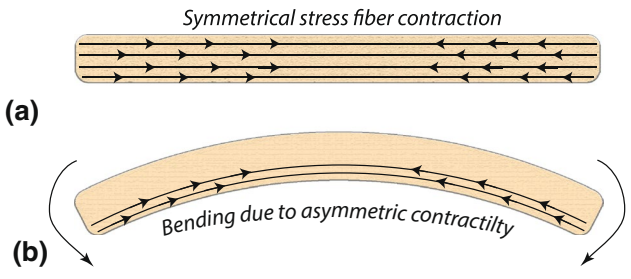

Fig. 6 **a** Symmetric contraction of stress fibers stiffens but does not bend ECs. **b** Asymmetric contraction of stress fibers causes stiffening and bending of ECs

3. *Model 2:* Due to the considerations above, in Model 2 we allow both rotation and axial motion of the EC ends. Furthermore, in Model 2 we implement the asymmetrical contraction of the stress fibers by allowing them to contract by various percentages; again these contractions are consistent with a variety of experimental reports noted above (Drenckhahn and Wagner 1986; Franke et al. 1984; Nehls and Drenckhahn 1991). These features of Model 2 are illustrated in Fig. 6b; we implement this in the FEM model by treating one half of the EC along its length to act as a contractile strip. Such asymmetrical contraction indeed induces bending and leads to the opening of slit caliber, but also causes the closing of adjacent slits, as described below.

   In both models, it should be noted that the ECs are treated as essentially incompressible and as the results will illustrate this leads to an interesting bounding, with respect to material and structural properties, of the extent of slit opening.

4.4 Simulation goals and expectations

Simulations were carried out using our WSM model and a model in which $L_{EC} = 8\mu$m; EC lengths of $\mathcal{O}(\sim 8\mu$m) are suggested by the SEM images of Fujita (1974) and Gálfiová et al. (2009), discussed above. A range of physiological relevant values for cell mechanical properties and driving pressures were used to explore the possible range of forecasted IES calibers, specifically to assess what is believed to be the observed range of $\mathcal{O}(0.8-1.5\,\mu$m). Particular focus was placed on the role of asymmetrical SF contraction on IES caliber and the causes of the experimentally observed asynchronous IES opening.

5 Simulation results

5.1 Results: Model 1

Figure 7 shows two views of the sinus and IES expansion based on our Model 1 and 1a design and using our WSM that takes $L_{EC} = 16\mu$m; note that the effects of uniform stress fiber contraction are also described; see also Supplementary Movie 1. Specific results for estimated slit caliber based on the maximum slit opening are listed in Table 2. We recall that to the maximum IES opening displacement, δ_s, we must impose the δ_s^0 due to axisymmetric sinus opening under the all-around pulling pressure P_{pull} to arrive at a total IES opening of $\delta_s = \delta_s^0 + \delta_s^b$; this is explained in Section 4.

Table 2 shows results for a range of pulling pressures, P_{pull}, that clearly indicates a natural progression of slit caliber with increasing P_{pull}. We note that, without stress fiber contraction, δ_s may reach values in the range 1.3μm to which δ_s^0 must be added; hence, total calibers in access of 1.8−1.9 μm are thereby envisioned. We note, however, that

Table 2 Models 1 and 1a results: $L_{EC} = 16\mu$m

EC modulus (kPa)	P_{pull} mmHg (Pa)	EC contraction (%)	δ_s^b (μm)
10	0.5 (66.7)	0	0.53
10	1.0 (133.3)	0	0.97
10	1.5 (200.0)	0	1.32
With uniform stress fiber contraction			
10	0.5 (66.7)	5	0.97
10	1.0 (133.3)	10	0.74
10	1.0 (133.3)	20	0.48
10	1.5 (200.0)	30	0.34

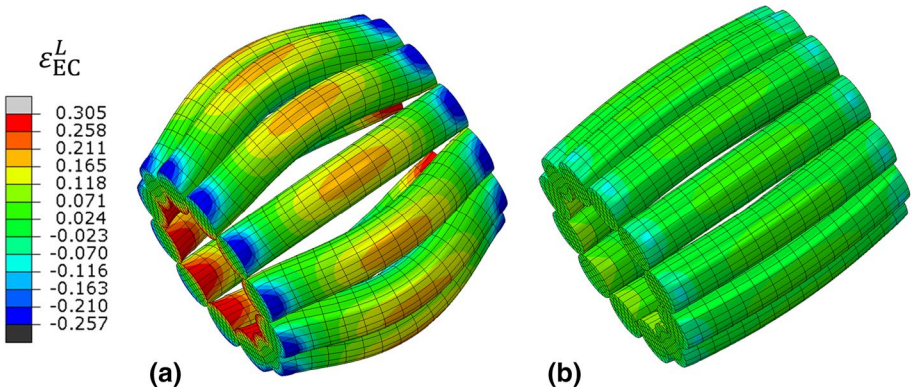

Fig. 7 Two views of a deformed sinus under the conditions of Model 1 with $L_{EC} = 16\,\mu$m and EC modulus taken as 10 kPa. **a** Distribution of longitudinal strain along the ECs (ϵ_{EC}^L) under $P_{pull} = 0.5$ mmHg (66.7 Pa) with no stress fiber contraction. **b** Distribution of longitudinal strain along the ECs (ϵ_{EC}^L) under $P_{pull} = 1.5$ mmHg (200 Pa) with an imposed 20% uniform stress fiber contraction. See more Model 1 and 1a results shown in Tables 2 and 3

this is strongly mitigated by the action of stress fiber uniform contraction as in Model 1a. With uniform stress fiber contraction, there is a monotonic trend of decreasing caliber as shown. Nonetheless, the total calibers predicted with the WSM that sets $L_{EC} = 16\,\mu m$ are rather large and generally may slightly exceed the expected range of 1−1.5 µm; based on the SEM evidence discussed above, we then used a value of $L_{EC} = 8\,\mu m$. We kept the EC-D at 3 µm for this larger set of simulations. Results for such cases are shown in Table 3.

Table 3 Model 1 and 1a results: $L_{EC} = 8\mu m$

EC modulus (kPa)	P_{pull} mmHg (Pa)	EC contraction (%)	δ_s^b (µm)
2.5	0.5 (66.7)	0	0.25
2.5	1.5 (200.0)	0	0.78
2.5	2.0 (266.6)	0	1.07
5	0.5 (66.7)	0	0.13
5	1.5 (200.0)	0	0.37
5	3.0 (400.0)	0	0.78
10	0.5 (66.7)	0	0.069
10	1.5 (200.0)	0	0.19
10	3.0 (400.0)	0	0.37
With uniform stress fiber contraction			
2.5	1.5 (200.0)	5	0.64
5	3.0 (400.0)	5	0.78
10	1.5 (200.0)	5	0.19
5	3.0 (400.0)	10	0.54
10	3.0 (400.0)	10	0.25
5	3.0 (400.0)	20	0.40
10	3.0 (400.0)	20	0.18
5	3.0 (400.0)	30	0.31

The results shown in Table 3 cover a wide range of P_{pull} and percentage of stress fiber contraction as well as the stiffness of the ECs.

The results of Model 1a with $L_{EC} = 8\,\mu m$ expectedly demonstrate reduced slit caliber with $0.5\,mmHg \le P_{pull} \le 3.0\,mmHg$, yet with EC modulus $E \sim 2.5\,kPa$ predicted slit calibers of $\mathcal{O}(1\,\mu m)$ are attained with $P_{pull} \sim 1.5{-}2\,mmHg$. Uniform stress fiber contraction results in expected EC stiffening and reduced calibers for the entire, we believe, physiologically relevant range of physical properties used. We again make note that to these δ_s^b calibers, we would add $\delta_s^0 \sim 0.5{-}0.7\,\mu m$, suggesting a total IES caliber of $\mathcal{O}(1{-}1.5\mu m)$.

5.2 Results: Model 2

Representative results using Model 2, which implements asymmetrical stress fiber contraction, are shown in Fig. 8 and Table 4; here again $L_{EC} = 8\mu m$. Model 2 reveals, most clearly, the role of stress asymmetrical fiber contraction on asynchronous as well as the role of EC near incompressibility.

In simulations, such as illustrated in the snapshots of Fig. 8 and Supplementary Movie 2, asymmetrical SF contraction was implemented in various ways that resembled a stochastic activation, e.g., selected ECs were allowed to undergo an asymmetrical SF contraction. In simulations, as shown in Fig. 8 the pattern of SF contraction involved SFs on adjacent ECs contracting asymmetrically to various

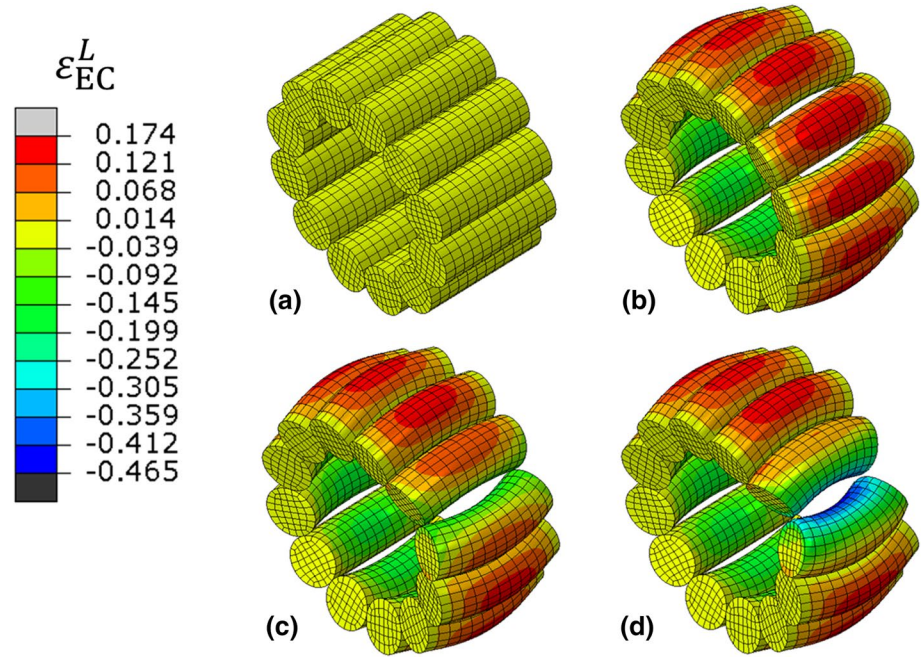

Fig. 8 Views of a deformed sinus under the conditions of Model 2 with $L_{EC} = 8\,\mu m$ and EC modulus taken as 10 kPa. **a** Original sinus section under zero load with no stress fiber contraction. **b** Distribution of longitudinal strain along the ECs (ϵ_{EC}^{L}) under $P_{pull} = 1.5\,mmHg$ (200.0 Pa) with no stress fiber contraction. **c, d** Distribution of longitudinal strain along the ECs (ϵ_{EC}^{L}) under $P_{pull} = 1.5\,mmHg$ (200.0 Pa) with an imposed 10% and 30% asymmetric stress fiber contraction, respectively, in a pair of neighboring ECs. See more Model 2 results shown in Table 4

Table 4 Model 2 results: $L_{EC} = 8\mu m$ (with asymmetrical stress fiber contraction)

EC modulus (kPa)	P_{pull} mmHg (Pa)	EC contraction (%)	δ_s^b (μm)
10	1.5 (200.0)	0	0.48
10	1.5 (200.0)	5	0.71
10	1.5 (200.0)	10	0.91
10	1.5 (200.0)	20	1.08
10	1.5 (200.0)	30	1.16
Higher P_{pull}			
10	2.0 (266.6)	0	0.63
10	2.0 (266.6)	10	0.95
10	2.0 (266.6)	20	1.19
10	2.0 (266.6)	30	1.22
Reduced EC modulus			
5	1.0 (133.3)	0	0.63
5	1.0 (133.3)	10	0.95
5	1.0 (133.3)	20	1.19
5	1.0 (133.3)	30	1.22
Higher P_{pull} and reduced EC modulus			
5	1.5 (200.0)	0	0.88
5	1.5 (200.0)	10	0.96
5	1.5 (200.0)	20	1.13
5	1.5 (200.0)	30	1.22
5	2.0 (266.6)	0	1.07
5	2.0 (266.6)	10	0.92
5	2.0 (266.6)	20	0.94
5	2.0 (266.6)	30	1.02

percentages. We hypothesize, however, that this type of pattern may not be unusual since as Chen and Weiss (1973) have pointed out "the slits are closed except when penetrated by blood cells, platelets, or macrophages." Hence, this sort of cooperative activation of asymmetrical SF contraction in adjacent ECs may be preferred and induced by signaling of impinging RBCs; singling may involve, for example, ATP emission by RBCs (Ellsworth et al. 2016; Sprague and Ellsworth 2012; Sprague et al. 1998).

It should be also noted that as a slit opens adjacent slits tend to close as the the adjacent ECs being pushed sideways cause an inevitable impingement of the ECs; it is this feature that helps explain the asynchronous IES activation observed by MacDonald et al. (1987), Groom et al. (2002). The process is a natural steric effect of cells undergoing impingement due to bending and via Poisson contraction.

Moreover, we note that since the ECs are nearly incompressible, the compression induced by SF contraction and bending tend to limit the extent to which IESs can open. This may be appreciated by examining at the trend in forecasted δ_s^b with increasing P_{pull} and/or with decreasing EC modulus E. We find, in fact, that δ_s^b essentially saturates at a level of $\mathcal{O}(\sim 1\,\mu m)$. If we then add $\delta_s^0 \sim 0.5{-}0.7\,\mu m$, we estimate that IES calibers of greater than $1.5{-}1.7\,\mu m$ may be difficult to achieve. Moreover, we again emphasize that IESs of a given section of sinus will inevitably open in the asynchronous manner we have demonstrated and in the manner directly visualized, in vivo, by MacDonald et al. (1987), Groom et al. (2002).

6 Discussion

6.1 General comments

Our paradigm and simulations demonstrate how the transient pressures within the red pulp, P_p, may mediate time-dependent calibers of the venous IESs and generally open the IESs despite the prevailing state where $P_p > P_s$. However, the asynchronous caliber behavior among the IESs of a given sinus must depend on mechanisms other than P_p or even $\Delta P_s = P_p - P_s$. Based on our paradigm, we hypothesize that stress fiber (SF) contractility within individual ECs may mediate the opening of individual IESs for times set by SF "activation." Stress fibers are reported to be activated by several stimuli including ATP-Mg^{++} (Drenckhahn and Wagner 1986) or shear forces associated with shear flows (Franke et al. 1984). The most likely cause of the transient opening and closing of IESs would then appear to be ATP activation, possibly by ATP emission by impinging red cells awaiting IES passage. This may be so since activation by shear flow would seem perhaps to act more symmetrically, whereas ATP emission may be more localized by particular cells impinging on certain IESs. Drenckhahn and Wagner (1986) report that ATP activation—that induced EC bending and general cell shape alterations—occurred within timescales of $\mathcal{O}(1{-}3\,s)$, but the temporal behavior of such ATP activation, viz. during fluctuations in ATP concentration, is as yet unknown. Interestingly, and perhaps directly relevant here, are the observations of spontaneous asymmetric EC bending (i.e., bulging) into the lumen of capillaries in a rat spleen that, in such cases, caused complete blockage of red cell flow for times of $\mathcal{O}(\sim 20s)$; it is suspected that stress fiber contraction was responsible for this transient occurrence (Ragan et al. 1988).

ATP release from erythrocytes has been studied extensively in recent years as it has been identified as an important singling event in the microvasculature that participates in mediating vasodilation (Ellsworth et al. 1995; Dietrich et al. 2000; Ellsworth et al. 2016; Sprague and Ellsworth 2012; Sprague et al. 1998). In this, the role and degree of deformation have been hypothesized to control shear-induced ATP release (Sprague et al. 1998; Price et al. 2004). Wan et al. (2008) used a microfluidic approach to study shear-induced

ATP release from human erythrocytes with temporal resolution of milliseconds. They formulated a mechanistic framework involving the retraction of the spectrin–actin skeleton and membrane deformation that revealed at least two timescales, both of which within the times scale of red cell IES transit. Hence, we again suggest that ATP release could be a factor mediating stress fiber contraction (Drenckhahn and Wagner 1986) and in the manner of ATP release from RBCs (Ellsworth et al. 1995; Dietrich et al. 2000). Likewise, ATP release from red cells has been studied in a wide range of deformation scenarios (Marginedas-Freixa et al. 2018; Mancuso et al. 2018). Still another attractive mechanism is the enhanced ATP release following deformation induced activation of Piezo1 and Ca^{++} uptake discussed by Cinar et al. Cinar et al. (2015).

6.2 Future research

The analysis presented herein suggests a number of areas for future research that would add vital additional insight and veracity to the predicted results. We list a few below.

1. *Red pulp modeling* A holistic fibrous-porous, viscoelastic, model of the reticular meshwork of the red pulp is needed to better assess the pulp pressure P_p and to provide a more quantitative framework for assessing red cell sequestration, including sequestration due to red cell adhesion to the meshwork. Such a model would provide the basis for a more quantitative description of open flow through the spleen. Such understanding would also provide more insight into determining the red cell IES transit kinetics by providing a more accurate specification of what we have called the IES transit driving force $\Delta P_s = P_p - P_s$. We estimated ΔP_s to be in the range 130–200 Pa by an analysis of the known rheology of the red pulp (Groom et al. 2002) in Section 3.3, and we noted that this along with the IES caliber would mediate red cell-slit transit times; our estimates of median transit times of 0.1–0.2 s were based on the video microscopy of MacDonald et al. (1987) and are what was estimated by the model simulations of, for example, Zhu et al. (2017) or Asaro and Zhu (2020). We recognize, however, that actual transit times are indeed mediated by both ΔP_s and slit caliber in general.

   Expanded insight into the flow of red blood cells into the red pulp would also provide needed background to evaluate the hypothesis of Klei et al. (2020) regarding lysis along with our paradigm (Asaro et al. 2020) for the mechanisms inducing membrane disruption, vesiculation, and lysis. Klei et al. (2020) found that red pulp macrophages (RPMs) do not appear to phagocytose intact senescent RBCs in vivo as Gottlieb et al. (2012) found they did not in vitro; rather, in analyzing RPMs taken from human spleens, they found that RPMs phagocytose RBC ghost cells produced via the process of hemolysis. Hence, we suggest that the adhesion of senescent RBCs to the red pulp and sinuses under shear flow may promote hemolysis via the mechanisms described by Asaro et al. (2020). To understand this, a more quantitative description of red cell flow through the red pulp is required.
2. *Sinus structural refinement* In our modeling of the sinus structure, certain approximations were necessarily made; some of these are readily remedied, yet others require more fundamental research. For example, the ring fibers were modeled as being essentially rigid except for their axisymmetric expansion, yet given the expected, and simulated, bending deflections this assumption does not appear critical; it would be a minor refinement to provide the ring fibers with more flexibility as more insight to their properties was known. A more important effect, however, is that of the boundary conditions, and degrees of freedom, imposed or allowed at the ends of ECs.
3. *Contractility of the EC stress fibers* The contractile behavior of the EC stress fibers clearly requires far more detailed study. Our paradigm has led, via our simulations, to an explanation of the observations of MacDonald et al. (1987) of both asynchronous and transient opening of IESs; one mechanism for these effects involves stress fiber contractility. It is known that induction of stress fibers in human endothelial cells may be triggered by ATP (e.g., Drenckhahn and Wagner 1986) and by shear forces imposed during shear flow (e.g., Franke et al. 1984). If more were known, quantitatively, about the effects of such influences, and since such flows can in fact be simulated, it would be possible to provide a more complete and quantitative picture of IES transit kinetics to compare to the video microscopy of MacDonald et al. (1987). Studies of contractility should attempt to measure contraction forces, possibly by recording cell deflections after documenting cell stiffness, e.g., via AFM probes.

   We also recall that the reticular meshwork itself is described as being contractile, especially in mammals such as the dog (Blue and Weiss 1981); to a much lesser extent, the meshwork of the human spleen may also be contractile. Contractility of the attached meshwork could also play a role in sinus expansion and IES opening, even in an asymmetric fashion; this too requires further investigation.

6.3 The role of RBC IES passage

The role of the spleen as a "filter" of blood is beyond contestation, yet the role of the IES slits of the venous sinuses may still require further elucidation. A variety of model

simulations have shown that RBC geometry (i.e., sphericity and size) plays a dominant role in determining whether the IES slit geometry at its maximum opening allows RBC passage per se (Asaro et al. 2018, 2020; Pivkin et al. 2016; Asaro and Zhu 2020). That this is expected to be the case is readily appreciated by noting that since the RBC's membrane is area incompressible, as is its volume, as a cell loses membrane and becomes more spherical, it loses the ability to alter its shape; recall that a sphere is the 3-D shape that minimizes the surface to volume ratio and as a near sphere, a cell loses its ability to change shape. Hence, as cells age, or vesiculate for other reasons such as storage or disease, and lose membrane area and volume, and become more spherical, reduced "deformability" and the inability to alter shape is axiomatic; that is, if changing shape is taken as the definition of "deformability." With adhesion being another key factor affecting RBCs, especially at different disease states or with ageing, the situation becomes more complicated and adhesion may play the dominant role.

Among mammals, humans, rats, and dogs possess sinusal spleens, but cats, horses, pigs, mice, and cows do not, yet the spleens all function as blood "filters." As noted by Schmidt et al. (1993), and as modeled herein, the walls of the sinusal spleen consist of long spindle-shaped endothelial cells held together by reticular, i.e., ring, fibers within which slits may open to allow red cell passage, involving considerable deformation. In contrast, the walls of pulp venules of the mouse or cat, as examples, are lined with smooth flattened irregularly shaped endothelial cells and have few and irregularly distributed openings, i.e., true fenestrations, in their walls (Scmidt et al. 1993; Hataba et al. 1981). Moreover as noted by Scmidt et al. (1993), and others such as Hataba et al. (1981), "The sizes of the fenestrations are mostly large enough to allow unimpeded entry of red cells in the walls" (Scmidt et al. 1993). As noted in Section 1, although red cells only make "occasional passages" through the IESs of the human (sinusal) spleen, the deformations they undergo strongly promote vesiculation; this was explained by Asaro et al. (2018) who also experimentally demonstrated that deformations produced in simple, yet tailored but unconstrained, oscillatory shear flows that closely resemble those that occur during IES passage indeed induce vesiculation. Asaro et al. (2020) went further and provided a paradigm for vesiculation in general forms of microcirculatory flows of the splenic-IES passage type. So the question arises: "Is a main function of splenic-IES passage, and hence the sinuses per se, to induce vesiculation in red cells compromised physiologically by aging, storage followed by transfusion, the formation of intracellular inclusions (Koyama et al. 1964), and various forms of ROS generation." It is, accordingly, believed that vesiculation occurs in the spleen (Bosman et al. 2012)—where rapid removal of toxic vesicles is facilitated—and we speculate that the images of small transparent "vesicles" found by Fujita (1974) are in fact vesicles formed during IES passage, see white arrow highlights in Fig. 9. Fujita did tentatively identify the discernable particles among these in the size range of $\mathcal{O}(\sim 150-1000\,\text{nm})$ as vesicles. We note that the extracellular vesicles imaged by Fujita Fujita (1974) do not appear to be the micropinocytotic vesicles reported by (Chen and Weiss 1972). They may, however, be the remenants of red cell lysis as hypothesized by Klei et al. (2020) and Asaro et al. (2020). Still other insight may be gained by considering the splenic role in diseased states; we conclude with two examples.

Southeast Asian ovalocytosis (SAO) is an inherited asymptomatic disorder characterized by cells with ovular shape and increased membrane stiffness (Safeukui et al. 2018); importantly, such cells are not spherical. The molecular basis for the increased membrane rigidity is traced to mutant SAO band 3 that leads to increased attachment to the skeleton and band 3 oligomerization (Liu et al. 1995, 1990). SAO cells are found to circulate freely in the vasculature and apparently are not unduly sequestered in the spleen although they display reduced "deformability" (Safeukui et al. 2018). Safeukui et al. (2018) found that by inducing various degrees of increased membrane stiffness in RBCs with diamide (dRBCs), that leads to increased protein–protein interactions and aggregation, the so-treated RBCs were preferentially sequestered in perfused human spleens, yet not nearly so "blocked" by a microbead filtering bed. Based on our current findings of how the IES slits of the human (or rat) spleen function, however, we may wonder if conditions that prevailed in their perfusion experiments, including the levels and time sequence of perfusion pressures, were a mediating factor. On the other hand, they logically surmised "that increased membrane rigidity per se might not markedly reduce the ability of RBCs to traverse the spleen" (Safeukui

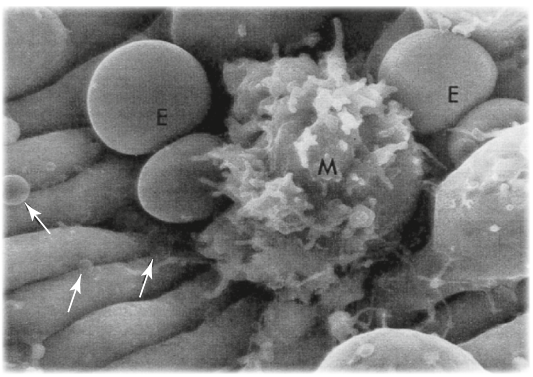

Fig. 9 SEM image taken from Fujita (1974) showing transparent vesicles (white arrows) aggregated around a human splenic sinus. The size range of those vesicles visible was in the range 150−1000 nm

et al. 2018). Alternatively, treatment with diamide may indeed induce the activation of adhesion receptors that lead to adhesion of dRBCs to the fibers of the red pulp reticular meshwork or to the sinus endothelium and subsequently to their clearance by RPMs.

The role of the human spleen in malaria may be somewhat different and complex. For *Plasmodium falciparum* malaria-infected RBCs (iRBCs), adhesion plays the dominant role in vascular or splenic sequestration of late stage iRBCs (Lee et al. 2019; Lim et al. 2020; Henry et al. 2020). For early stage iRBCs when adhesion is not considered a major factor (Henry et al. 2020), splenic sequestration is enhanced by at least two factors, viz. the inability to freely transit the IESs due to their decreased surface-to-volume ratio (Henry et al. 2020) and increased membrane shear modulus of iRBCs (Mills et al. 2007; Huang et al. 2013; Henry et al. 2020). During acute malaria, increased clearance of all RBCs (infected and uninfected) has been found (Henry et al. 2020), while increased iRBC stiffness was found for both infected and uninfected RBCs as well (Mills et al. 2007; Huang et al. 2013). Causes of increased membrane shear modulus were found to be due to interactions between the parasite and the RBC skeleton (Mills et al. 2007; Sisquella et al. 2017). Henry et al. (2020) also note that a potential role of IES passage may include "pitting" of the resident parasite, in line with our mention, above, of a similar role in the removal of inclusions. Hence, the role of the spleen in malaria-infected cells is rather complex and continued efforts are required to more thoroughly understand the overall interaction between parasitized RBCs and the human spleen in malaria.

Hence, when taken together with the findings of Klei et al. (2020, 2018), and the fact that only a subpopulation of mammals possess sinusal spleens, we wonder if the main function of the IESs within the splenic sinuses may be to provide for self-protection via deformation-assisted vesiculation. Here, *self-protection* refers to the removal of damaged molecular material such as oxidized hemoglobin in the manner described by, e.g., Willekens et al. (2003a, b) and by Bosman et al. (2005), or via the pitting function mentioned above. Cell clearance per se by simple "blocking" of RBCs may not be the primary splenic sinus-IES function. It is curious, albeit anecdotal, that Blue and Weiss (1981) report that in the sinusoidal spleens of the dog, red cells are often seen "trapped" within the IESs with their main body on the lumen side, but rarely with their main body on the pulp side. This is seen in the images of MacDonald et al. (1987) as shown in Fig. 2d; we now realize that this "trapping" is most plausibly due to adhesion (Asaro et al. 2020). This again shows the importance of taking adhesion into careful consideration in determining the spleen's overall filtering function and the role IESs would actually play.

Supplementary Information The online version contains supplementary material available at https://doi.org/10.1007/s10237-021-01503-y.

Acknowledgements M.D. acknowledges support from NIH R01HL154150.

Author contributions R.J. Asaro, M. Dao, and I. MacDonald all contributed to and performed the research and the writing of this paper.

References

Abraldes JG, Sarlieve P, Tandon P (2014) Measurement of portal pressure. Clin Liver Dis 18:779–792

Alberts B, Johnson A, Lewis J, Raff M, Roberts K, Walter P (2002) The Cell. Garland Science

Allarg A, Schiffelers RM, van Solinge WW, van Wijk R (2013) Red blood cell vesiculation in herditaryhemolytic anemia. Front Physiol 4:1–15

Asaro RJ, Lubarda VA (2006) Mechanics of solids and materials. Cambridge Univ Press, New York

Asaro RJ, Zhu Q (2020) Vital Erythrocyte phenomena: what can theory, modeling, and simulation offer? Biomech Model Mechanobiol. https://doi.org/10.1007/s10237-020-01302-x

Asaro RJ, Zhu Q, Cabrales P (2018) Erythrocyte Aging, Protection via Vesiculation: an analysis methodology via oscillatory flow. Front Physiol 9:1607

Asaro RJ, Zhu Q, MacDonald IC (2020) Tethering, evagination, and vesiculation via cell-cell interactions in microvascular flow. Biomech Model Mechanobiol 20:31–53

Atkinson M, Sherlock S (1954) Intraspleenic pressure as index of portal venous pressure. Lancet 1954:1325–1327

Bauer K, Kratzer M, Otte M, de Quintana KL, Hagmann J, Arnold GJ, Eckerskorn C, Lottspeich F, Siess W (2000) Blood 96:4236–4245

Biosfleury A, Mohandas N (1977) Anti-body-induced spherocytic anemia II. Splenic passage and sequestration of red cells. Blood Cells 3:197–208

Blue J, Weiss L (1981) Electron microscopy of the red pulp of the dog spleen including vascular arrangements, periarterial macrophage sheaths (ellipsoids), and the contractile, innervated reticular meshwork. Am J Anat 161:189–218

Bonomini M, Sirolli V, Gizza F, Di Stante S, Grilli A, Felaco M (2002) Enhanced adhesion of human uremic eruthrocytes to vascular endothelium: role of phosphatidylserine exposure. Kidney Int 62:1358–1363

Bosman GJ, Willekens FL, Werre JM (2005) Erythrocyte aging: a more than superficial resemblance to apoptosis? Cell Physiol Biochem 16(1–3):1–8

Bosman G, Willekens FLA, Weere JM (2012) Erythocyte Senesecence. In: Land F, Föller M (eds) Erythrocytes, physiology and pathophysiology. Imperial College Press, London

Carlson BM (2018) The human body: linking structure and function. Academic Press, New York

Cesta MF (2006) Normal structure, function, and histology of the spleen. Taxicol Pathol 34:455–465

Chen LT, Weiss L (1972) Electron microscopy of the red pulp of human spleen. Am J Anat 134:425–458

Chen LT, Weiss L (1973) The role of the sinus wall in the passage of erythrocytes through the spleen. Blood 41:529–537

Cho Y, De Bruyn PPH (1975) Passage of red blood cells through the sinusoidal wall of the spleen. Am J Anat 142:91–106

Ciana A, Achilli C, Gaur A, Minetti G (2017a) Membrane remodeling and vesicle formation during ageing of human red blood cells. Cell Physiol Biochem 42:1127–1138

Ciana A, Achilli C, Minetti G (2017b) Spectrin and other membrane-skeletal components in human red blood cells of different age. Cell Physiol Biochem 42:1139–1152

Cinar E, Zhou S, DeCourcey J, Wang Y, Waugh RE, Wan J (2015) Peizo1 regulates mechanotransductive release of ATP from human RBCs. PNAS 112:11783–11788

Closse C, Dochary-Prigent J, Boisseau MR (1999) Phosphatidylserine-related adhesion of human erythrocytes to vascular endothelium. Br J Haematol 107:1365–2141

Dietrich HH, Ellsworth ML, Sorague RS, Dacey RG (2000) Red blood cell regulation of microvascular tone through adenosine triphosphate. Am J Physiol Heart Circul Physiol 278(2):H1294–H1298

Diez-Silva M, Dao M, Han J, Lim C-T, Suresh S (2010) Shape and biomechanical characteristics of human red blood cells in health and disease. MRS Bull 35:382–388

Diez-Silva M, Park Y, Huang S, Bow H, Mercereau-Puijalon O et al (2012) Pf155/RESA protein influences the dynamic microcirculatory behavior of ring-stage Plasmodium falciparum infected red blood cells. Sci Rep 2:614–620

Drenckhahn D, Wagner J (1986) Stress fibers in the splenic sinus endothelium in situ: molecular structure, relationship to extracellular matrix, and contractility. J Cell Biol 102:1738–1747

Ellsworth ML, Forrester T, Ellis CG, Dietrich HH (1995) The erythrocyte as a regulator of vascular tone. Am J Physiol 269(6–2):H2155

Ellsworth ML, Ellis CG, Sprague RS (2016) Role of erythrocyte-released ATP in the regulation of microvascular oxygen supply in skeletal muscle. Acta Physiol 216(3):265–276

Essler M, Retzer M, Bauer M, Heemskerk JW, Aepfelbacher M, Siess W (1999) Mildly oxidized low density lipoprotein induces contraction of human endothelial cells through activation of Rho/Rho kinase and inhibition of myosin light chain phosphatase. J Biol Chem 274(43):30361–30364

Fens MHAM, van Eijk R, Andringa G, van Rooijen KL, Dijstelbloem HM, Rasmussen JT, de Vooght KMK, Schiffelers RM, Gaillard CAJM, van Solinge WW (2012) A role for activated endothelial cells in red blood cell clearance: implications for vasopathology. Haematologica 97(4):500–508

Franke RP, Grate M, Schnitter H, Seiffge D, Mittermayer C (1984) Induction of human vascular endothelial stress fibers by fluid shear stress. Nature 307:648–649

Fujita T (1974) A scanning electron microscope study of the human spleen. Arch Histol Jap 37:187–216

Gálfiová P, Varga I, Kopáni M, Michalka P, Michalová J, Jakubovský J, Polák S (2009) Some possibilities of representing microcirculation in human spleen. Biologia 64(6):1242–1246

Gottlieb Y, Topez O, Cohen LA, Yakov LD, Haber T, Morgenstern A, Weiss A, Berman KC, Meyron-Holtz E (2012) Physiologically aged red blood cells undergo erythrophagocytosis in vivo but not in vitro. Haematologica 97(7):994–1002

Groom AC, MacDonald IC, Schmidt EE (2002) Splenic microcirculatory blood flow and function with respect to red blood cells. In: Bowdler AJ (ed) The complete speen. Humanna Press, Totowa, pp 23–50

Hataba Y, Kirino Y, Suzuki T (1981) Scanning electron microscopic study of the red pulp of mouse spleen. J Electr Microsc 30:46–56

Henry B, Roussel C, Carucci M, Brousse V, Ndour PA, Buffet P (2020) The human spleen in malaria: filter of shelter? Trends Parasitol 36:435–446

Huang S, Undisz A, Diez-Silva M, Bow H, Dao M, Han J (2013) Dynamic deformability of Plasmodium falciparum-infected erythrocytes exposed to artesunate in vitro. Integrat Biol 5(2):414–422

Kang I, Panneerselvam D, Panoskaltis VP, Eppel SJ, Marchant RE, Doerchuk CM (2008) Changes in the hyperelastic properties of endothelial cells induced by tumor necrosis factot-α. Biophys J 94:3273–3285

Kataoka N, Iwaki K, Hashimoto K, Mochizuki S, Ogasawara Y, Sato M, Tsujioka K, Kajiya F (2008) Measurements of endothelial cell-to-cell and cell-to-substrate gaps and micromechanical properties of endothelial cells during monocyte adhesion. PNAS 99:15638–15643

Klei TRL, de Back DZ, Asif PJ, Verkuijlen PJJH, Veldthuis M, Ligthart PC, Berghuis J, Clifford E, Beuger BM, van den Berg TK, van Zwieten R, El Nemar W, van Bruggen R (2018) Glycophorin-C sialylation regulates Lu/BCAM adhesive capacity during erythrocyte againg. Blood Adv 2:14–24

Klei TRL, Dalimot J, Nota B, Veldthuis M, Mul FPJ, Rademakers T, Hoogenboezem M, Nagelkerke SQ, van IJcken WFJ, Oole E, Scendsen P, Moestrup SK, van Alphen FPJ, Meijer AB, Kuijpers TW, van Zwieten R, van Bruggen R (2020) Hemolysis in the spleen drives erythreocyte turnover. Blood 136(14):1579–1589

Koyama S, Aoki S, Deguchi K (1964) Electron microscopic observation of the splenic red pulp with special reference to the pitting function. Mie Med J 14:143–188

Leal JKF, Adjobo-Hermans MJW, Bosman GJCM (2018) Red blood cell homeostasis: mechanisms and effects of microvesicle generation in health and disease. Front Physiol 9:703

Lee W-C, Russell B, Rénia L (2019) Sticking for a cause: the falciparum malaria parasites cytoadherence paradigm. Front Immunol 10:01444

Levesque MJ, Groom AC (1976) Washout kinetics of red cells and plasma from the spleen. Am J Physiol 231:1665–1671

Li H, Lu L, Li X, Buffet PA, Dao M, Karniadakis GE, Suresh S (2018) Mechanics of diseased red blood cells in human spleen and consequences for hereditary blood disorders. Proc Natl Acad Sci USA 115(38):9574–9579

Lim YB, Thingna J, Kong F, Dao M, Cao J, Lim C-T (2020) Temperature-induced catch-slip to slip bond transit in plasmodium falciparum-infected erythrocytes. Biophys J 118(1):105–116

Liu SC, Zhai S, Palek J, Golan DE, Amato D et al (1990) Molecular defect of the band 3 protein in Southeast Asian Ovalocytosis. J N Engl Med

Liu SC, Palek J, Yi SJ, Nichols PE, Derick LH et al (1995) Molecular basis of alterewd red blood cell membrane properties in Southeast Asian Ovalocytosis: role of the mutant band 3 protein in band 3 oligomerization and retention by the membrane skeleton. Blood 86:349–358

Low PS, Waugh SM, Zinke K (1985) The role of hemoglobin denaturation and band 3 clustering in red cell aging. Science 227:531–533

Lutz HU (2004) Innate immune and non-immune mediators of erythrocyte clearance. Cell Mol Biol (Noisy-le-grand) 50(2):107–116

Lutz HU, Bogdanova A (2013) Mechanisms tagging senescent red blood cells for clearance in healthy humans. Front Physiol 4:1–15

MacDonald IC, Ragan DM, Schmidt EE, Groom AC (1987) Kinetics of red blood cell passage through interendothelial slits into venous sinuses in rat spleen, analyzed by in vivo microscopy. Microvasc Res 33:118–134 (**See also videos on youtube.com**)

MacDonald IC, Schmidt EE, Groom AC (1991) The high splenic hematocrit: a rheological consequence of red cell flow through the reticular meshwork. Micrvasc Res 42:60–76

Mancuso JE, Jayaraman A, Ristenpart WD (2018) Centrifugation-induced release of ATP from red blood cells. PLOS 13(9):e0203270

Marginedas-Freixa I, Alvarez CL, Moras M, Leal Denis MF, Hattab C et al (2018) Human erythrocytes release ATP by a novel pathway involving VDAC oligomerization independent of pannexin-1. Sci Rep 8:11384

Mebius R, Kraal G (2005) Structure and function of the spleen. Nat Rev Immunol 5:606–616

Mills JP, Diez-Silva M, Quinn DJ, Dao M, Lang MJ, Tan KSW, Lim C-T, Milon G, David PH, Mercereau-Puijalon O, Bonnefoy S, Suresh S (2007) Effect of plasmodial RESA protein on deformability of human red blood cells harboring Plasmodium falciparum. Proc Natl Acad Sci USA 104(22):9213–9217

Miyoshi M, Fujita T (1971) Stero-fine structure of the splenic red pulp. A combined scanning and transmission electron microscope study on dog and rat spleen. Arch Histol Jap 33:225–246

Mohandas N, Gallagher PG (2008) Red cell membrane: past, present, and future. Blood 112:3939–3948

Mohanty JG, Nagababu E, Rifkind JM (2014) Red blood cell oxidative stress impairs oxygen delivery and induces red blood cell aging. Front Physiol 5:1–6

Nehls V, Drenckhahn D (1991) Demonstration of actin filament stress fibers in microvascular endothelial cells in situ. Microvasc Res 42:103–112

Opdyke DF (1993) Hemodynamics of blood flow though the spleen. Am J Physiol 219(1):102–106

Opdyke DF, Apostolico R (1966) Splenic contraction and optical density of blood. Am J Physiol 211:329–334

Pandey KB, Rizvi SI (2010) Markers of oxidative stress in erythrocytes and plasma during aging in humans. Oxid Med Cell Longev 3(1):2–12

Pandey KB, Rizvi SI (2011) Biomarkers of oxidative stress in red blood cells. Biomed Pap Med Fac Univ Palacky Czeh Rep 155(2):131–136

Pernow J, Mahdi A, Yang J, Zhou Z (2019) Red blood cell dysfunction: a new player in cardiovascular disease. Cardiovasc Res 115:1596–1605

Pivkin IV, Peng Z, Karniadakis GE, Buffet PA, Dao M, Suresh S (2016) Biomechanics of red blood cells in human spleen and consequences for physiology and disease. Proc Natl Acad Sci USA 113(28):7804–7809

Price AK, Fisher DJ, Martin RS, Spence DM (2004) Deformation-induced release of ATP from erythrocytes in a poly(dimethylsiloxane)-based microchip with channels that mimic resistance vessels. Anal Chem 76:4849–4855

Ragan DMS, Schmidt EE, MacDonald IC, Groom AC (1988) Spontaneous cyclic contractions of the capillary wall in vivo, impeding red cell flow: a quantitative analysis. Microvasc Res 36:13–30

Sadd MH (2005) Elasticity: theory, applications and numerics. Elsveier, Oxford

Safeukui I, Buffet PA, Deplaine G, Perrot S, Brousse V, Ndour A, Nguyen M, Mercereau-Puijalon O, David PH, Milon G, Mohandas N (2012) Quantitative assessment of sensing and sequestration of spherocytic erythrocytes by the human spleen. Blood 120(2):424–430

Safeukui I, Buffet PA, Deplaine G, Perrot S, Bouusse V et al (2018) Sensing of red blood cells with decreased membrane deformability by the human spleen. Blood Adv 2:2581–2587

Saito H, Yokoi Y, Watanabe S, Tajima J, Kuroda H, Namihisa T (1988) Reticular meshwork of the spleen in rats studied by electron microscopy. Am J Anat 181:235–252

Sato H, Katano M, Takigawa T, Masuda T (2001) Estimation for the elasticity of vascular endothelial cells on the basis of atomic force microscopy and Young's modulus of gelatin gels. Polym Bull 47:375–381

Schmidt EE, MacDonald IC, Groom AC (1988) Microcirculatory pathways in normal human spleen, demonstrated by scanning electron microscopy of corrosion casts. Am J Anat 181:253–266

Schmidt EE, MacDonald IC, Groom AC (1993) Comparative aspects of splenic microcirculatory pathways in mammals: the region bordering the white pulp. Scanning Microsc 7:613–628

Shah R, Patel T, Freedman JE (2018) Circulating extracellular vesicles in human disease. N Engl J Med 379:958–966

Shen Q, Wu MH, Yuan SY (2009) Endothelial contractile cytoskeleton and microvascular permeability. Cell Health Cytoskelet 1:43–50

Sisquella X, Nebi T, Thompson JK, Whitehead L, Malpede BM et al (2017) Plasmodium falciparum ligand binding to erythrocytes induce alterations in deformability essential for invasion. eLife 6:21083–21094

Song SH, Groom AC (1971) The distribution of red cells in the spleen. Am J Physiol Pharmacol 49:734–743

Song SH, Groom AC (1972) Sequestration and possible maturation of reticulocytes in the normal spleen. Can J Physiol Pharmacol 50:400–406

Song SH, Groom AC (1974) Scanning electron microscope study of the splenic red pulp in relation to the sequestration of immature and abnormal red cells. J Morphol 144:439–452

Sprague RS, Ellsworth ML (2012) Erythrocyte-derived ATP and perfusion distribution: role of intracellular and intercellular communication. Microcirculation 19(5):430–439

Sprague RS, Ellsworth ML, Stephenson AH, Kleinhenz ME, Lonigro AJ (1998) Deformation-induced ATP release from red blood cells requires CFTR activity. Am J Physiol Heart C 275:H1726-171732

Steinger B, Bette M, Schwarzbach H (2011) The open microcirculation in human spleens: a three-dimensional approach. J Histochem Cytochem 59(6):639–648

Thomas CE (1967) An electron- and light-microscope study of sinus structure in perfused rabbit and dog spleens. Am J Anat 120:527–552

Wan J, Ristenpart WD, Stone HA (2008) Dynamics of shear-induced ATP release from red blood cells. PNAS 105:16432–16437

Wautier JL, Paton RC, Wautier MP, Pintigny D, Abadie E, Passa P, Caen JP (1981) N Engl J Med 305:237–242

Wautier JL, Wautier MP (2013) Molecular basis of erythrocyte adhesion to endothelial cells in disease. Clin Hemotol Microcircul 53(1–2):11–21

Wautier JL, Wautier MP, Schmidt AM, Anderson CM, Hori O, Zoukourian C, Capron L, Chappey O, Yan SD, Brett J (1994) Advanced glycation end products (AGEs) on the surface of diabetic erythrocytes bind to the vessel wall via a specific receptor inducing oxidant stress in vasculature: a link between surface-associated AGEs and diabetic complications. Proc Natl Acad Sci USA 91:7742–7746

Wautier MP, Héron E, Picot J, Colin Y, Hermine O, Wautier JL (2011) Red blood phosphatidylserine exposure is responsible for increased erythrocyte adhesion to endothelium in central retinal vein occlusion. J Throm Haemostatis 9(5):1049–1055

Willekens FLA, Weere JM, Groenen-döpp YA, Bregt-Roerdinkholder B, de Pauw B, Bosman GJCGM (2003a) Erythrocyte vesiculation: a self-protective mechanism? Br J Haematol 141:549–556

Willekens FLA, Bregt-Roerdinkholder B, Groenen-döpp YA, Bos HJ, Bosman GJCGM, van den Bos AG, Verkeij AJ, Weere JM (2003b) Haemoglobin loss from erythrocytes in vivo results from spleen-facilitated vesiculation. Blood 101:747–751

Zhu X, Han W, Wang L, Chu H, Zhao J, Xu Y, Wang T, Guo W (2015) Penicillar arterioles of red pulp in residual spleen after subtotal splenectomy due to splenomegaly in cirrhotic patients: a comparative study. Int J Clin Pathol 8(1):711–718

Zhu Q, Salehyar S, Cabrales P, Asaro R (2017) Prospects of human erythrocyte skeleton-bilayer dissociation during splenic flow. Biophys J 113(4):900–912

Zimring JC (2020) Turning over a new leaf on turning over RBCs. Blood 136(14):1569–1570

Erythrocyte flow through the interendothelial slits of the splenic venous sinus

Ming Dao[1] · Ian MacDonald[2] · R. J. Asaro[3]

[1] Department of Materials Science and Engineering, Massachusetts Institute of Technology, Cambridge, MA 02139, USA

[2] Department of Medical Biophysics, Schulich School of Medicine and Dentistry Western University, London, ON, Canada

[3] Department of Structural Engineering, University of California, San Diego, La Jolla, CA 92093, USA

Supplementary Information

Supplementary Movie 1: Deformation of a sinus section under the conditions of Model 1 with the endothelial cell (EC) modulus taken as 10 kPa and $L_{\mathrm{EC}} = 16$ μm. The evolution of the longitudinal strain along the ECs ($\varepsilon_{\mathrm{EC}}^{L} = \mathrm{LE33}$) is shown first under P_{pull} = 0 - 0.5 mmHg (0 - 66.7 Pa) with no stress fiber contraction, followed by adding 0 to 20% *uniform stress fiber contraction* in all ECs while holding P_{pull} = 0.5 mmHg (66.7 Pa).

Supplementary Movie 2: Deformation of a sinus section under the conditions of Model 2 with the endothelial cell (EC) modulus taken as 10 kPa and $L_{\mathrm{EC}} = 8$ μm. The evolution of the longitudinal strain along the ECs ($\varepsilon_{\mathrm{EC}}^{L} = \mathrm{LE33}$) is shown first under P_{pull} = 0 - 1.5 mmHg (0 - 200.0 Pa) with no stress fiber contraction, followed by adding 0 to 30% *asymmetric stress fiber contraction* in two neighboring ECs while holding P_{pull} = 1.5 mmHg (200.0 Pa).